Supplementary Information for:

Ligand Field Strength Mediates Electron Delocalization in Octahedral [(HL)2Fe6(L')m]n+ Clusters

Raúl Hernández Sánchez, Shao-Liang Zheng and Theodore A. Betley*

Department of Chemistry and Chemical Biology, Harvard University,

12 Oxford Street, Cambridge, Massachusetts 02138 USA.

E-mail: betley@chemistry.harvard.edu

Table of Contents

Experimental section

Fe₂Mes₄. FeCl₂ (6.0 g, 47.3 mmol) was suspended in 60 mL of THF in a round flat-bottom flask. The head space was evacuated and the flask heated to 80 °C for 20 min. This was allowed to stir for one hour at room temperature and subsequently MesMgBr (94.7 mL, 1 M, 94.7 mmol) was added slowly at 0.5 mL/min. Last, 20 mL of 1,4-dioxane were added and the reaction mixture stirred for 4 h. The resulting dark red solution was filtered in a 150 mL medium porosity frit with celite and washed with THF. The filtrate was dried overnight under vacuum. The red solid product was re-dissolved in diethyl ether and filtered again in the same way. The filtrate was concentrated to ~90 mL and cooled down to −35 °C. Bulk crystallization occurs within two days (7.26g first crystallization, 52%). Recrystallization was carried out to improve purity (6.28 g, 45%). The ¹H NMR in C₆D₆ matches that previously reported.[1]

Near Infrared Spectroscopy. Spectra were collected in 1 mm path length cuvettes on a Perkin Elmer Lambda 750 spectrometer at room temperature. All solutions were prepared in the glovebox and the cuvettes sealed with a Teflon tape and cap. Absorbance values were kept under 1 for all concentrations measured.

Data was plotted as "reduced" absorption (ε/ν versus ν), as recommended by D'Alessandro and Keene for charge transfer bands.[2] Igor Pro (Wavemetrics) was used to fit the intervalence charge transfer (IVCT) bands to a Gaussian function. From the fits (to the ε/ν versus ν spectra) the peak maximum position, ν_{max}; molar absortivity, ε_{max}; and the full-width-at-half-maximum, $\Delta\nu_{1/2}$, were obtained. Several methods were employed, as described in the main text, to calculate the electronic coupling H_{ab}. The first makes use of the Hush formula Eq. S.1.[3] The second method used considers the thermodynamic parameters extracted from the electrochemical data. As described by Brunschwig and Sutin[4] the free energy of the comproportionation reaction to form the mixed valence product can be described by Eq. S.2; where $\Delta G_{nr}°$ includes all the nonresonance contributions, and $\Delta G_r°$ contains only the electronic interaction by delocalization. The nonresonance contributions are generally small, especially if $\Delta E_{1/2}$ is large. Thus, it is assumed $\Delta G_c° \approx \Delta G_r°$. This free energy for a partially delocalized species is given by Eq. S.3 and for a fully delocalized by Eq. S.4.[4] The third method used to classify the extent of delocalization

is based on the predicted and experimental IVCT bandwidths according to Eq. S.5.[5] The calculated electronic coupling, H_{ab1} and H_{ab2}; and classification parameter Γ are presented in the main text, Table 3.

$$H_{ab1} = \frac{2.06 \ \text{x}10^{-2} \left(v_{max} \varepsilon_{max} \Delta v_{1/2} \right)^{1/2}}{r_{ab}} \qquad \text{Eq. S.1}$$

$$\Delta G_c^\circ = \Delta G_{nr}^\circ + \Delta G_r^\circ \qquad \text{Eq. S.2}$$

$$-\Delta G_c^\circ \approx -\Delta G_r^\circ = \frac{2H_{ab}^2}{v_{max}} \qquad \text{Eq. S.3}$$

$$-\Delta G_c^\circ \approx -\Delta G_r^\circ = 2\left(H_{ab} - \frac{v_{max}}{4} \right) \qquad \text{Eq. S.4}$$

$$\Gamma = 1 - \frac{\Delta v_{1/2}}{\Delta v_{1/2}^\circ} \quad \left(\Delta v_{1/2}^\circ = \sqrt{16RT_{298 \ K} v_{max} \ln 2} \right) \qquad \text{Eq. S.5}$$

Magnetometry. Data was collected as described in the main text. Two methods were employed to analyze the data. The first one considers the six metal-atom cluster making up a single spin (SS) as employed previously.[6] The second considers an exchange interaction between each adjacent (J_{cis}) and *trans*-located (J_{trans}) pair of iron atoms in the octahedral core. A similar treatment has been employed before for octahedral hexamanganese clusters.[7] The Hamiltonian in Eq. S.6 describes the exchange interactions in an octahedral arrangement of metal ions.
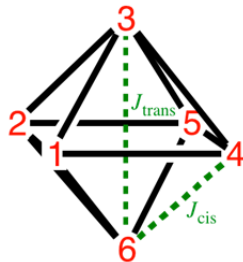
$$\hat{H} = -2J_{cis}\begin{pmatrix}\hat{S}_1\cdot\hat{S}_2 + \hat{S}_1\cdot\hat{S}_3 + \hat{S}_1\cdot\hat{S}_4 + \hat{S}_1\cdot\hat{S}_6 + \hat{S}_2\cdot\hat{S}_3 + \hat{S}_2\cdot\hat{S}_5 \\ +\hat{S}_2\cdot\hat{S}_6 + \hat{S}_3\cdot\hat{S}_4 + \hat{S}_3\cdot\hat{S}_5 + \hat{S}_4\cdot\hat{S}_5 + \hat{S}_4\cdot\hat{S}_6 + \hat{S}_5\cdot\hat{S}_6\end{pmatrix} - 2J_{trans}\left(\hat{S}_1\cdot\hat{S}_5 + \hat{S}_2\cdot\hat{S}_4 + \hat{S}_3\cdot\hat{S}_6\right) \qquad \text{Eq. S.6}$$

$$\hat{S}_a = \hat{S}_1 + \hat{S}_5 \quad ; \quad \hat{S}_b = \hat{S}_2 + \hat{S}_4 \quad ; \quad \hat{S}_c = \hat{S}_3 + \hat{S}_6 \quad ; \quad \hat{S} = \hat{S}_a + \hat{S}_b + \hat{S}_c$$

$$\hat{H} = -J_{cis}\left(\hat{S}^2 - \hat{S}_a^2 - \hat{S}_b^2 - \hat{S}_c^2\right) - J_{trans}\left(\hat{S}_a^2 + \hat{S}_b^2 + \hat{S}_c^2 - \hat{S}_1^2 - \hat{S}_2^2 - \hat{S}_3^2 - \hat{S}_4^2 - \hat{S}_5^2 - \hat{S}_6^2\right) \qquad \text{Eq. S.7}$$

$$E = -J_{cis}\begin{bmatrix}S(S+1) - S_a(S_a+1) \\ -S_b(S_b+1) - S_c(S_c+1)\end{bmatrix} - J_{trans}\begin{vmatrix}S_a(S_a+1) + S_b(S_b+1) + S_c(S_c+1) \\ -S_1(S_1+1) - S_2(S_2+1) - S_3(S_3+1) \\ -S_4(S_4+1) - S_5(S_5+1) - S_6(S_6+1)\end{vmatrix} \qquad \text{Eq. S.8}$$

The Hamiltoninan in Eq. S.6 can be transformed into Eq. S.7 by using the Kambe vector coupling method[8] and the substitutions defined above for $\hat{S}_a$, $\hat{S}_b$, $\hat{S}_c$ and $\hat{S}$; where the latter is the total spin. From Eq. S.7 one can obtain the corresponding energy levels, Eq. S.8. By evaluating Eq. S.8 for each S and plugging that into the Van Vleck equation[9] one can derive an expression for χ_M vs. T. This expression contains from 20 to 2706 terms in the numerator (and similarly in the denominator) depending on the individual spins being considered, $\hat{S}_1$ to $\hat{S}_6$. Tables like the one derived by Hendrickson and Christou[7] for six Mn(III) were derived here for all the redox transfer isomers. A Matlab program was written to accomplish the latter calculation (see below). The individual spins were considered according to the following Scheme S1.
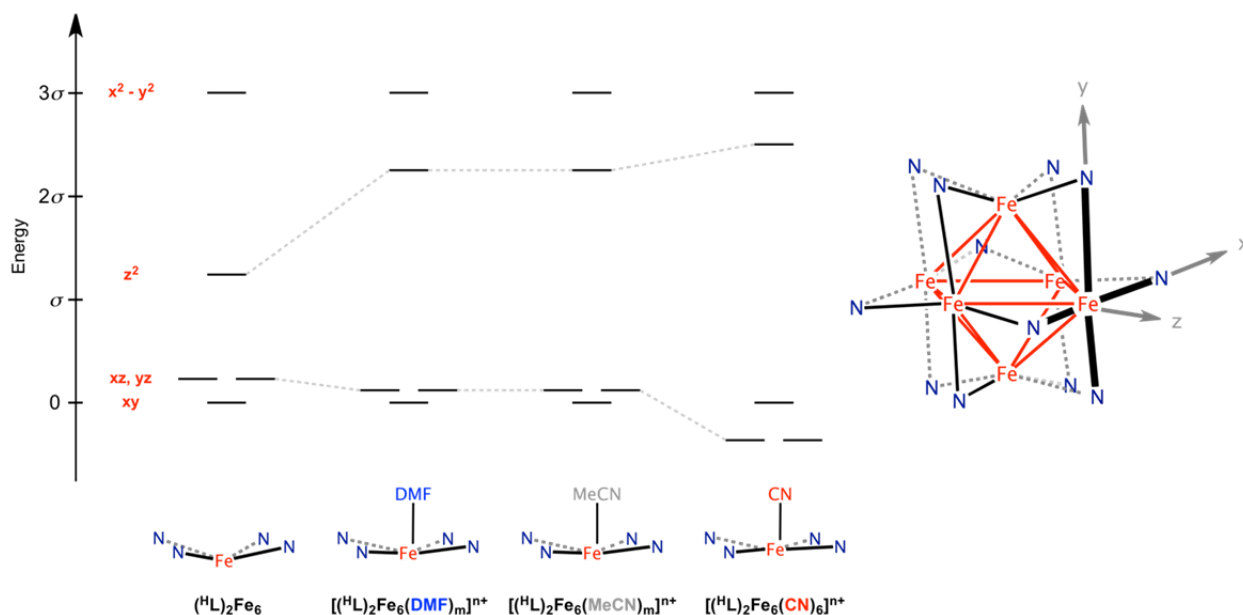
The relative energies of the frontier orbitals at each individual iron site, depicted in Scheme S1, were used as an approximation to deduce the potential spins states that could be achieved depending on the geometry and ligand bound at each iron site. The coordinate axis at each site was chosen as depicted above. In all cases the orbital with $d_{x^2-y^2}$ parentage was considered unpopulated. This was deduced primarily by comparing the average bond distances between the Fe and the bridging amides (see Table 1) to other maximally high-spin $S = 2$ Fe(II) sites in similar geometries.[10] The spin state considered for a formally Fe(II) residing in a four- or a five-coordinate site is in all cases $S = 1$. The formally Fe(III) site gives rise to $S = {}^3/_2$ if this resides on a four- or five-coordinate ligand environment with either DMF or MeCN bound; in contrast, if cyanide is bound a low-spin $S = {}^1/_2$ is considered.

These two methods were employed to fit and/or simulate the magnetic susceptibility data. It is important to remark that the assumptions made here may oversimplify the model to treat the data; especially in the dimethylformamide electron transfer series.

The variable-temperature, variable-field magnetization data was analyzed according to the spin Hamiltonian in Eq. S.9 using the software *PHI*.[11]

$$\hat{H} = D\hat{S}_z^2 + E\left(\hat{S}_x^2 - \hat{S}_y^2\right) + g\mu_B \boldsymbol{S} \cdot \boldsymbol{H} \tag{Eq. S.9}$$

Matlab code. The required equations to model the data via the coupled spin (CS) approach are:

$$J_{\text{cis}} \text{ coefficient } = \{S(S+1) - S_a(S_a+1) - S_b(S_b+1) - S_c(S_c+1)\} \tag{Eq. S.10}$$

$$J_{\text{trans}} \text{ coefficient } = \left\{ \begin{array}{l} S_a(S_a+1) + S_b(S_b+1) + S_c(S_c+1) \\ -S_1(S_1+1) - S_2(S_2+1) - S_3(S_3+1) \\ -S_4(S_4+1) - S_5(S_5+1) - S_6(S_6+1) \end{array} \right\} \tag{Eq. S.11}$$

$$\chi_M = \frac{N_A g^2 \mu_B^2}{3k_B T} \frac{\sum_i \text{NUM}_i \exp\left(-\frac{E_i}{k_B T}\right)}{\sum_i \text{DENOM}_i \exp\left(-\frac{E_i}{k_B T}\right)} + \text{TIP} \tag{Eq. S.12}$$

$$\text{NUM} = S(S+1)(2S+1) \tag{Eq. S.13}$$

$$\text{DENOM} = (2S+1) \tag{Eq. S.14}$$

The ultimate goal is to calculate χ_M for an initial set of parameters $\{S_{1\to6}$ ($\therefore S_{a\to c}$, and S), J_{cis}, J_{trans}, g, and TIP$\}$ which is then least-squared refined against the experimental data. The desired values to optimize are the exchange coupling constants J_{cis} and J_{trans}. To carry on this task the Van Vleck equation (Eq. S.12) was broken into individual contributions Eq. S.8, 10, 11, 13, and 14. First, calculation of total S was carried on for a given set of [S_a, S_b, S_c]. Each combination [S, S_a, S_b, S_c] was used to evaluate the corresponding coefficients of J_{cis}, and J_{trans} (Eq. S.10 and 11). Furthermore, having each [S, S_a, S_b, S_c] set of values allows for the evaluation of Eq. S.13 and 14. Each set of spin state values and coefficients were calculated in Matlab by the script *raul_magnetic.m* from which the code is reproduced below. The output of *raul_magnetic.m* is a .csv file, which contains a table where each line corresponds to: [S, S_a, S_b, S_c, J_{cis} coeff, J_{trans} coeff, NUM, DENOM].

raul_magnetic.m

```
function supermatrix = raul_magnetic(Sa,Sb,Sc)
%Set up all of the inital spins
Smax=Sa+Sb+Sc;
Smin=Smax-round(Smax-.5);
X=(Sa-round(Sa-.5)):1:Sa;
Y=(Sb-round(Sb-.5)):1:Sb;
I=(Sa+Sb-round(Sa+Sb-.5)):1:(Sa+Sb);
J=(Sc-round(Sc-.5)):1:Sc;

%Find the combinations (i,j) that work.
treetop=[];
for t=Smin:Smax
    for i=1:size(I,2)
        for j=1:size(J,2)
            if (I(i)+J(j))>=t
                if t>=abs(I(i)-J(j))
                treetop=[treetop; I(i),J(j),t];
                end
            end
        end
    end
end

%Decompose i into (x,y).
treemiddle=[];
for t=I
    for x=1:size(X,2)
        for y=1:size(Y,2)
            if (X(x)+Y(y))>=t
                if t>=abs(X(x)-Y(y))
                treemiddle=[treemiddle; X(x),Y(y),t];
                end
            end
        end
    end
end

%Find the right combinations.
treefull=[];
for z=1:size(treetop,1)
    i=treetop(z,1);
    for m=1:size(treemiddle,1)
        if treemiddle(m,3)==i
            treefull=[treefull; treemiddle(m,1), treemiddle(m,2), treetop(z,2), treetop(z,3)];
```

```
        end
    end
end

Jtrans=zeros(size(treefull,1),1);
Jcis=zeros(size(treefull,1),1);
num=zeros(size(treefull,1),1);
denom=zeros(size(treefull,1),1);
for f=1:size(treefull,1)
    a=treefull(f,1);
    b=treefull(f,2);
    c=treefull(f,3);
    st=treefull(f,4);
    Jtrans(f)=a*(a+1)+b*(b+1)+c*(c+1);
    Jcis(f)=st*(st+1)-(a*(a+1)+b*(b+1)+c*(c+1));
    num(f)=st*(st+1)*(2*st+1);
    denom(f)=2*st+1;
end
supermatrix=[treefull, Jcis, Jtrans, num, denom];
dlmwrite('Coefftable',supermatrix);
csvwrite(['A' int2str(Sa*10) 'B' int2str(Sb*10) 'C' int2str(Sc*10) '.csv'],supermatrix);
```

With this table in hand the evaluation and least-square refinement of the magnetic susceptibility can be accomplished. The least-square refinement was carried out employing the script *optimizechit.m*, which calls *raul_magnetic.m* for evaluation and once refinement is accomplished it runs *simchit.m* to plot the results. To run the optimization a file named <u>fitinput.csv</u> must be provided containing the experimental data in two columns [T (K), $\chi_M T$]. Simulation (without least-square refinement) of $\chi_M T$ for a given set of parameters can be accomplished by using the script *onlysimchit.m* (similarly it calls *raul_magnetic.m*).

optimizechit.m

```
function [james,SSresidmap,J]=optimizechit(Jcisstart,Jtransstart,Sa,Sb,Sc,giso,chiindep,B)
experimental = 'fitinput.csv';
[exper,delimiterOut]=importdata(experimental);
supermatrix = raul_magnetic(Sa,Sb,Sc);

niter=2;
stepcis=1;
steptrans=1;
rangecis=20;
rangetrans=20;
```

```
Jcis=Jcisstart;
Jtrans=Jtransstart;

tic
for q=1:niter
    cis=(Jcis-rangecis/2):stepcis:(Jcis+rangecis/2);
    trans=(Jtrans-rangetrans/2):steptrans:(Jtrans+rangetrans/2);
    SSresid=zeros(size(cis,2),size(trans,2));
    lowcoords=[0,0];
    lowSSresid=10^20;
    for c=1:size(cis,2)

        for t=1:size(trans,2)
            [~,SSresid(c,t)]=chit2(cis(1,c),trans(1,t),supermatrix,giso,chiindep,B,exper);
            if SSresid(c,t)<lowSSresid
                lowcoords=[c,t];
                lowSSresid=SSresid(c,t);
            end
        end

    end
    Jcisold=Jcis;
    Jtransold=Jtrans;
    Jcis=cis(1,lowcoords(1,1));
    Jtrans=trans(1,lowcoords(1,2));
    stepcis=0.5;
    steptrans=0.5;
    rangecis=2;
    rangetrans=2;
end
toc

james=[Jcis,Jtrans,lowSSresid];    %test1
SSresidmap=SSresid;                %test2
J=[cis;trans];                    %test3
constant = (giso^2)*0.125;
forplot=simchit(Jcis,Jtrans,exper(:,1),supermatrix,constant,chiindep,B,exper);
figure();
plot(exper(:,1),exper(:,2),exper(:,1),forplot);

dlmwrite('chitoutput_fit',forplot);
dlmwrite('Jcis-Jtrans-lowSSresid',james);
dlmwrite('3Dmap-SSresid',SSresidmap);
end
```
simchit.m

```matlab
function raul=simchit(Jcis,Jtrans,T,supermatrix,constant,chiindep,B,exper)
%Remeber to change the individual Si to account for the constant in the
%Jtrans term.
S1=0.5;
S2=0.5;
S3=0.5;
S4=0.5;
S5=0.5;
S6=0.5;
a=supermatrix(:,5);
b=supermatrix(:,6);
Sa=supermatrix(:,1);
num=supermatrix(:,7);
denom=supermatrix(:,8);
raul=zeros(size(T));
n=size(T,1);
ofterms=size(a,1);
k=0.69593476;
for l=1:n
   numsum=0;
   denomsum=0;
   for m=1:ofterms
      numtmp=num(m,1)*exp(1/k/T(l)*(a(m,1)*Jcis+(b(m,1)-S1*(S1+1)-S2*(S2+1)-S3*(S3+1)-
S4*(S4+1)-S5*(S5+1)-S6*(S6+1))*Jtrans-B*(supermatrix(m,4)+0.5)));
      dentmp=denom(m,1)*exp(1/k/T(l)*(a(m,1)*Jcis+(b(m,1)-S1*(S1+1)-S2*(S2+1)-
S3*(S3+1)-S4*(S4+1)-S5*(S5+1)-S6*(S6+1))*Jtrans-B*(supermatrix(m,4)+0.5)));

      numsum=numsum+numtmp;
      denomsum=denomsum+dentmp;
   end
   raul(l,1)=numsum/denomsum;
end

%match to fit data by multiplying by T to make XT and the constant out
%front
chiindep2=zeros(size(T));
for l=1:n
   indep=chiindep*exper(l,1);
   chiindep2(l,1)=indep;
end

raul=raul*constant + chiindep2;

end
```
onlysimchit.m

S13

```matlab
function raul=onlysimchit(Jcis,Jtrans,Sa,Sb,Sc,giso,chiindep,B)
%Remeber to change the individual Si to account for the constant in the
%Jtrans term.
S1=1.0;
S2=0.5;
S3=1.0;
S4=0.5;
S5=0.5;
S6=0.5;

tic
experimental = 'fitinput.csv';
[exper,delimiterOut]=importdata(experimental);
supermatrix = raul_magnetic(Sa,Sb,Sc);
T = exper(:,1);
a=supermatrix(:,5);
b=supermatrix(:,6);
Sa=supermatrix(:,1);
num=supermatrix(:,7);
denom=supermatrix(:,8);
raul=zeros(size(T));
n=size(T,1);
ofterms=size(a,1);
k=0.69593476;
constant = (giso^2)*0.125;
for l=1:n
    numsum=0;
    denomsum=0;
    for m=1:ofterms
        numtmp=num(m,1)*exp(1/k/T(l)*(a(m,1)*Jcis+(b(m,1)-S1*(S1+1)-S2*(S2+1)-S3*(S3+1)-
S4*(S4+1)-S5*(S5+1)-S6*(S6+1))*Jtrans-B*(supermatrix(m,4)+0.5)));
        dentmp=denom(m,1)*exp(1/k/T(l)*(a(m,1)*Jcis+(b(m,1)-S1*(S1+1)-S2*(S2+1)-
S3*(S3+1)-S4*(S4+1)-S5*(S5+1)-S6*(S6+1))*Jtrans-B*(supermatrix(m,4)+0.5)));
        %numtmp=num(m,1)*exp(1/k/T(l)*(a(m,1)*Jcis+(b(m,1))*Jtrans-
B*(supermatrix(m,4)+0.5)));
        %dentmp=denom(m,1)*exp(1/k/T(l)*(a(m,1)*Jcis+(b(m,1))*Jtrans-
B*(supermatrix(m,4)+0.5)));

        numsum=numsum+numtmp;
        denomsum=denomsum+dentmp;
    end
    raul(l,1)=numsum/denomsum;
end

%match to fit data by multiplying by T to make XT and the constant out
%front
```

```matlab
chiindep2=zeros(size(T));
for l=1:n
    indep=chiindep*exper(l,1);
    chiindep2(l,1)=indep;
end

raul=raul*constant + chiindep2;
figure();
plot(exper(:,1),exper(:,2),exper(:,1),raul);
toc
dlmwrite('Chit-simulation',raul);
end
```

Table S1. Crystallographic data for compounds **4 – 9**.

	4	**5**	**6**
Chemical formula	$C_{64}H_{92}F_{12}Fe_6N_{18}O_7P_2$	$C_{70}H_{104}F_{18}Fe_6N_{20}O_8P_3$	$C_{76}H_{118}B_4F_{16}Fe_6N_{22}O_{10}$
Formula weight	1850.60	2123.74	2182.26
Space group	$P2_1$	P-1	$P2_1/n$
***a* (Å)**	10.1978(9)	13.4702(13)	17.812(2)
***b* (Å)**	14.1321(13)	13.7249(13)	12.6705(15)
***c* (Å)**	25.820(2)	14.289(2)	20.346(2)
***α* (deg)**	90	102.518(2)	90
***β* (deg)**	95.3841(16)	111.315(2)	95.7441(19)
***γ* (deg)**	90	110.937(1)	90
***V* (Å^3)**	3704.6(6)	2108.2(4)	4568.7(9)
Z	2	1	2
μ (mm^{-1})	1.28	1.17	1.03
T (K)	100(1)	100(1)	100(1)
***R1*[a] (*wR2*[b])**	0.050 (0.124)	0.040 (0.100)	0.085 (0.199)
GoF	1.040	0.990	1.333
Reflections	13036	7963	8086
Radiation type	Mo $K\alpha$	Mo $K\alpha$	Mo $K\alpha$

[a]$R1 = [\Sigma w(F_o - F_c)^2/\Sigma wF_o^2]^{1/2}$; [b]$wR2 = [\Sigma[w(F_o^2 - F_c^2)^2]/\Sigma w(F_o^2)^2]^{1/2}]$, $w = 1/[\sigma^2(F_o^2) + (aP)^2 + bP]$, where $P = [\max(F_o^2,0) + 2(F_c^2)]/3$

	7	8	9
Chemical formula	$C_{88}H_{125}Fe_6N_{27}$	$C_{92}H_{132}Fe_6N_{24}$	$C_{56}H_{70}Fe_6N_{20}NaO_8$
Formula weight	1896.24	1909.32	1509.41
Space group	*C2/c*	*P2₁/c*	*P*-1
***a* (Å)**	15.345(3)	12.459(4)	11.3522(9)
***b* (Å)**	20.716(5)	17.980(5)	11.9330(9)
***c* (Å)**	29.732(7)	22.485(5)	12.6036(10)
***α* (deg)**	90	90	81.788(1)
***β* (deg)**	103.496(4)	113.923(13)	84.609(1)
***γ* (deg)**	90	90	64.472(1)
***V* (Å³)**	9191(4)	4604(2)	1523.9(2)
Z	4	2	1
μ (mm⁻¹)	0.98	0.98	1.47
T (K)	100(1)	100(1)	100(1)
***R1*ᵃ (*wR2*ᵇ)**	0.074 (0.182)	0.061 (0.144)	0.051 (0.142)
GoF	1.179	0.996	1.036
Reflections	8324	8217	6988
Radiation type	Mo $K\alpha$	Mo $K\alpha$	Mo $K\alpha$

[a]$R1 = [\Sigma w(F_o - F_c)^2/\Sigma wF_o^2]^{1/2}$; [b]$wR2 = [\Sigma[w(F_o^2 - F_c^2)^2]/\Sigma w(F_o^2)^2]^{1/2}]$, $w = 1/[\sigma^2(F_o^2) + (aP)^2 + bP]$, where $P = [\max(F_o^2,0) + 2(F_c^2)]/3$

Table S2. Half-wave potentials for the cyanide species $[(^HL)_2Fe_6(CN)_6]^{n-6}$ (simplified in the table as $[Fe_6]^{n-6}$) in solvents of varying dielectric constant (κ).

	Reduction Potentials vs (Fc/Fc$^+$)[a]							
κ [DN][b]	$[Fe_6]^0$	$\underset{-e^-}{\overset{+e^-}{\rightleftharpoons}}$	$[Fe_6]^-$ (K_c, 10^{12})	$\underset{-e^-}{\overset{+e^-}{\rightleftharpoons}}$	$[Fe_6]^{2-}$ (K_c, 10^{20})	$\underset{-e^-}{\overset{+e^-}{\rightleftharpoons}}$	$[Fe_6]^{3-}$
NMP[c] 32.5 [27.3]	0.27 (123)		−0.48 (112)	(6.80)	−1.70 (161)	(0.57)	
MeCN 36.6 [14.1]	0.4[d] (29)[e]		−0.39 (123)		−1.52 (77)	(0.23)	
DMF 38.2 [26.6]	---		−0.45 (83)		−1.66 (87)	(2.50)	
DMA 38.8 [27.8]	---		−0.52 (80)		−1.73 (82)	(4.70)	
PC[f] 66.1 [15.1]	0.33 (127)		−0.39 (113)	(1.70)	−1.53 (125)	(0.30)	

[a]Peak-to-peak potential in parenthesis (ΔE_p in mV). [b]Dielectric constant (κ) and donor number (DN). [c]Done at 300 mV/s. [d]Irreversible oxidation. [e]Upper limit. [f]Done at 200 mV/s.
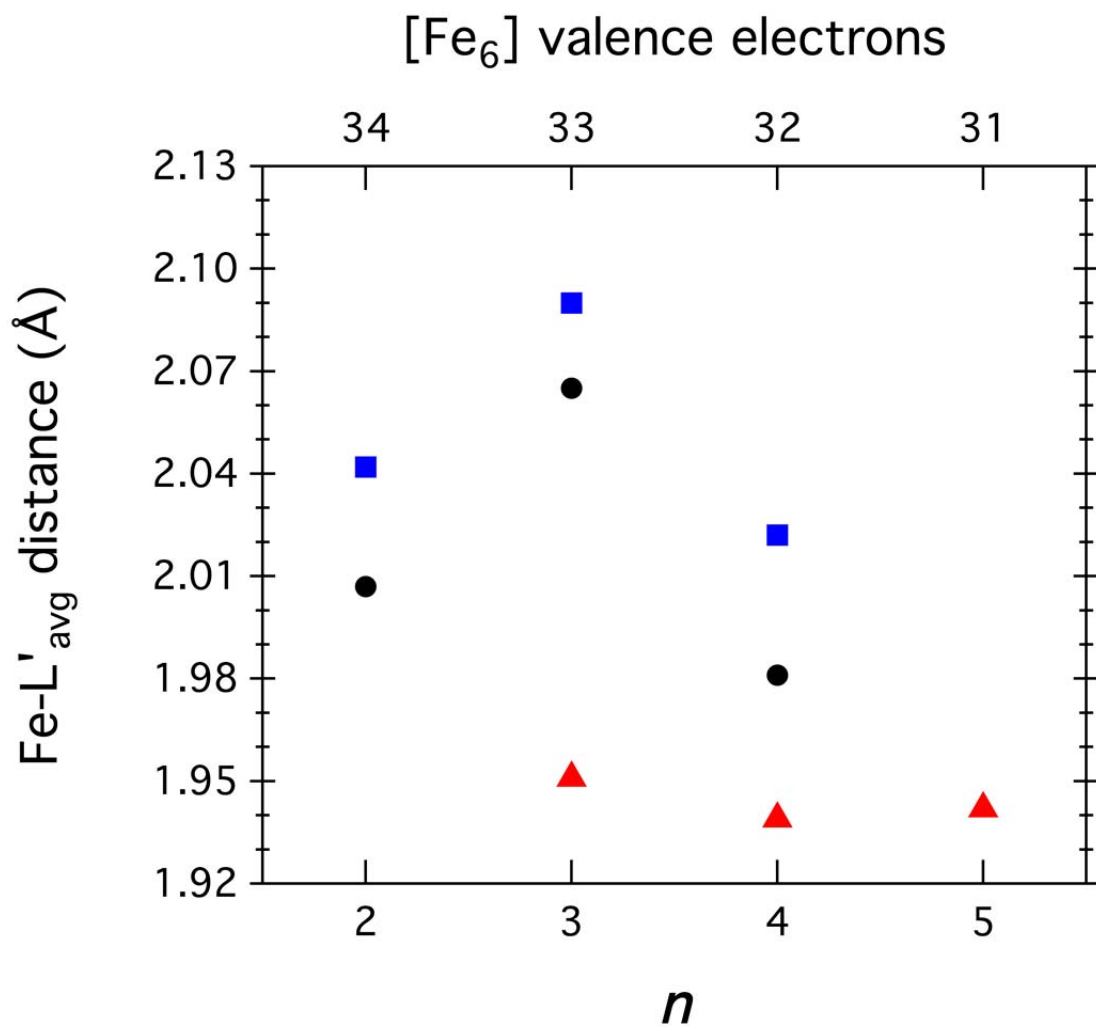
Figure S1. Average Fe–L' distances. $[(^HL)_2Fe_6(L')_m]^{n+}$: Fe–N for L' = MeCN (solid black circles, ●, **1 – 3**); Fe–O for L' = DMF (solid blue squares, ■, **4 – 6**). $[(^HL)_2Fe_6(CN)_6]^{n-6}$: Fe–C for L' = cyanide (solid red triangles, ▲, **7 – 9**).
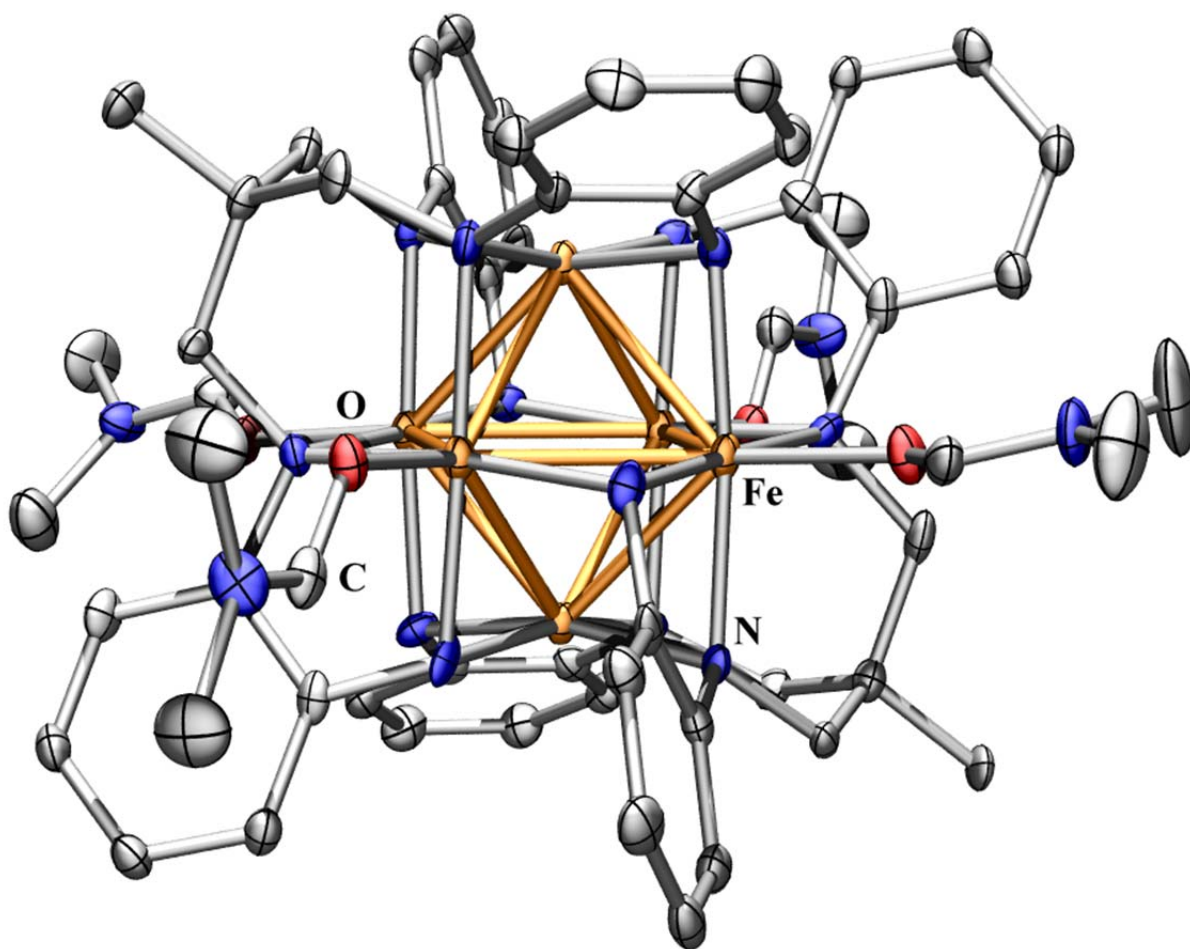
Figure S2. Solid state molecular structure of $[(^{H}L)_2Fe_6(DMF)_4]^{2+}$, cation of **4**. Thermal ellipsoids set at 50% probability level (hydrogen atoms omitted for clarity). Fe orange, C black, N blue, O red.
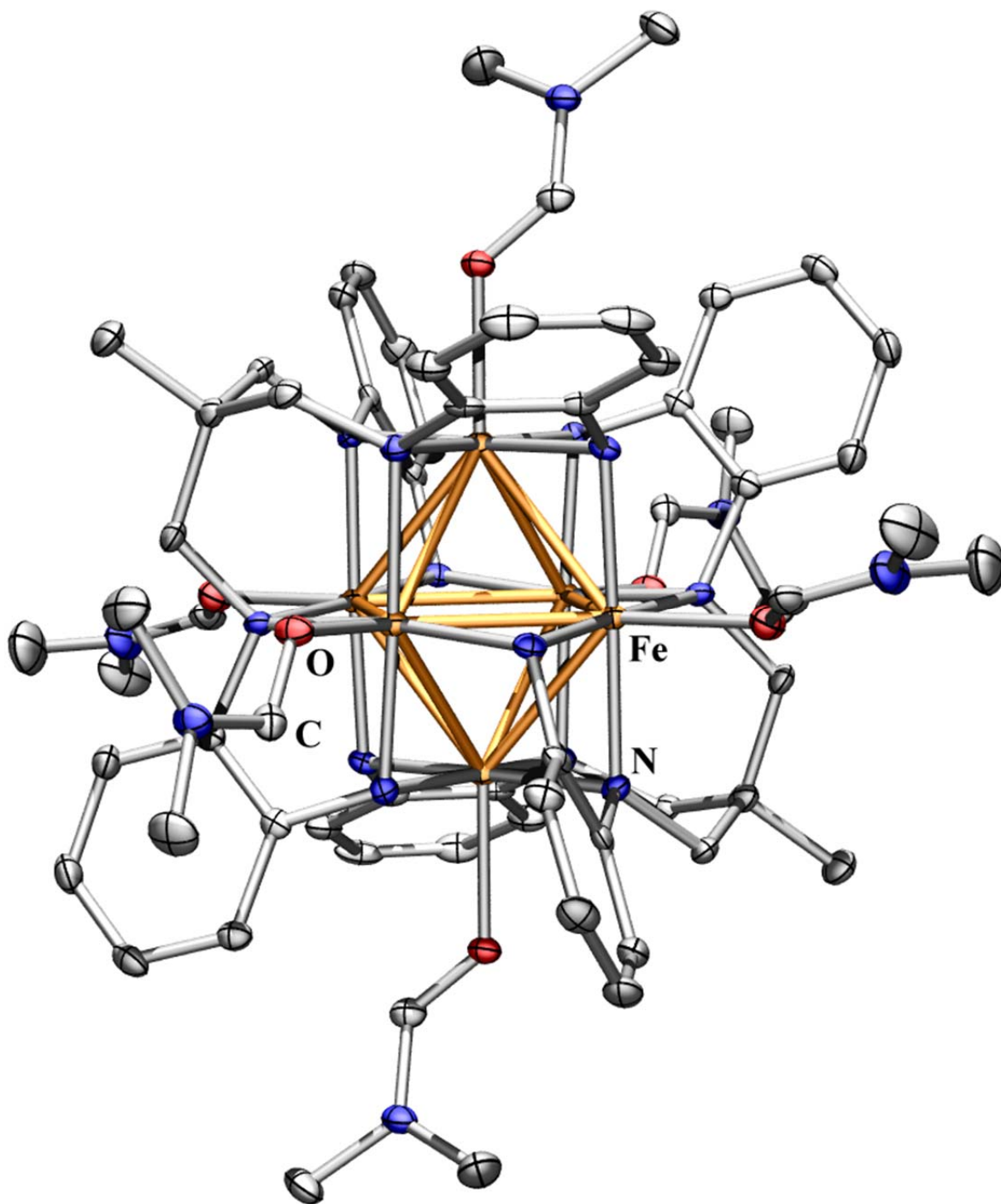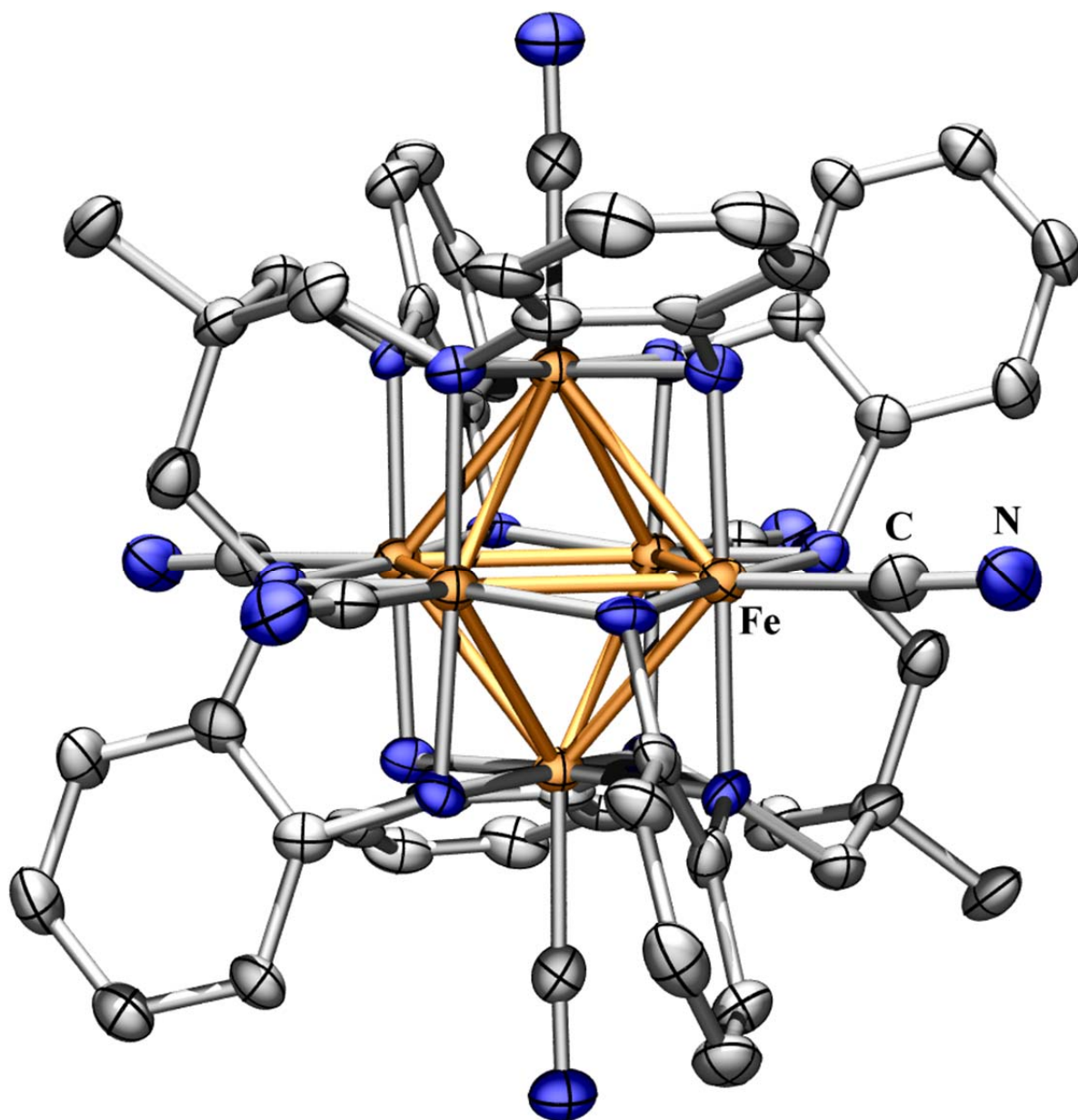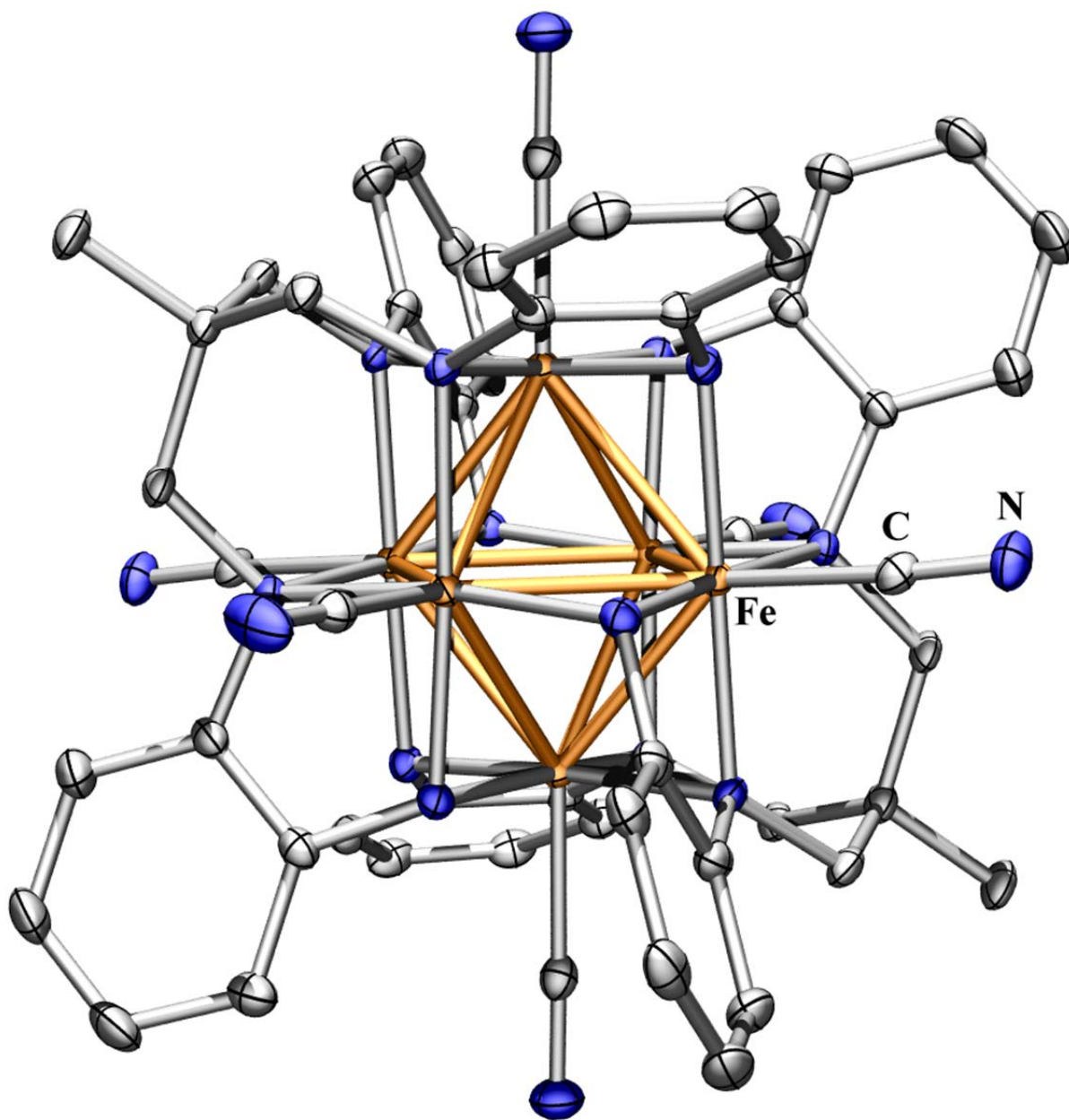
***Figure S3***. Solid state molecular structure of $[(^{H}L)_2Fe_6(DMF)_6]^{3+}$, cation of **5**. Thermal ellipsoids set at 50% probability level (hydrogen atoms omitted for clarity). Fe orange, C black, N blue, O red.
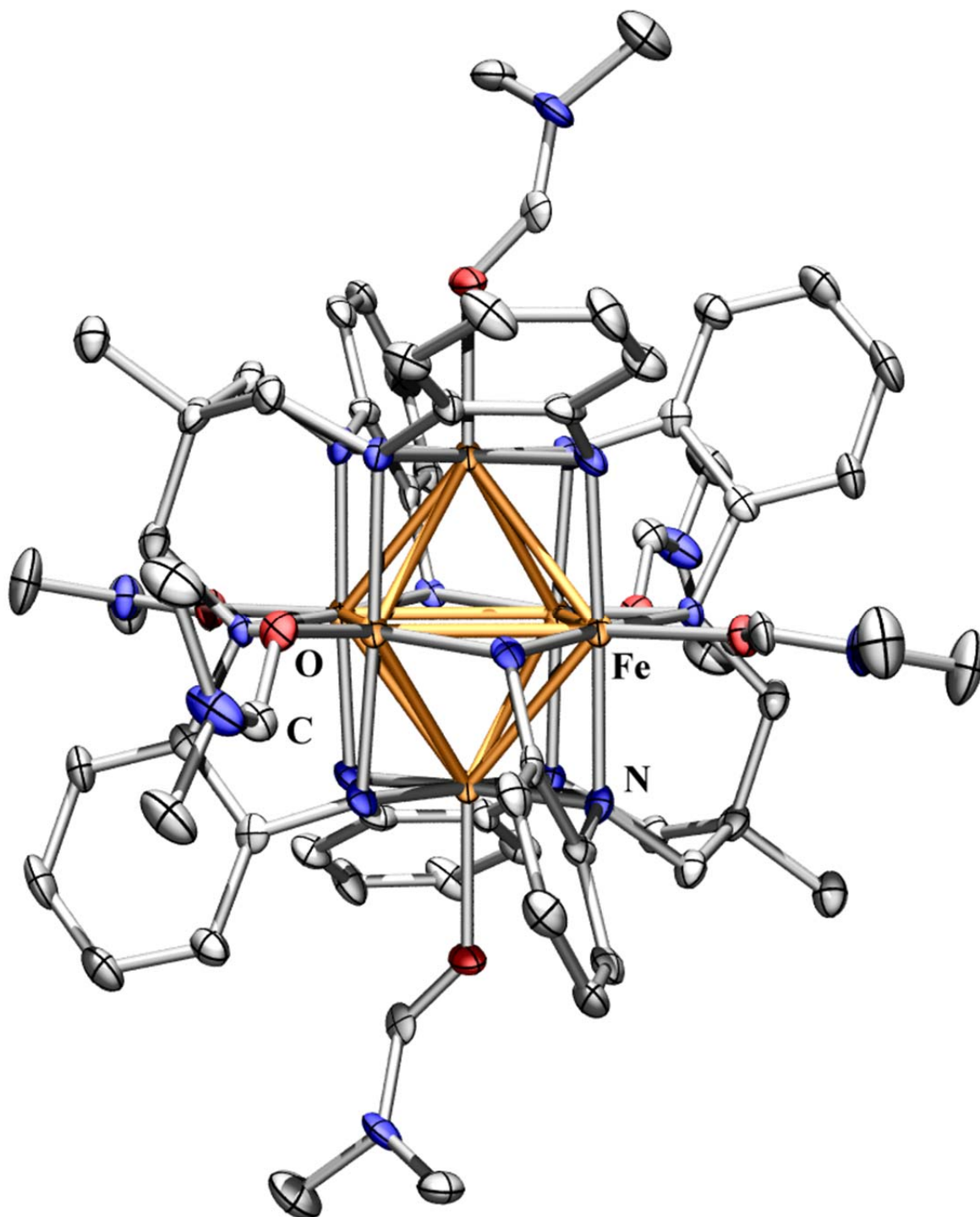
Figure S4. Solid state molecular structure of $[(^{H}L)_2Fe_6(DMF)_6]^{4+}$, cation of **6**. Thermal ellipsoids set at 50% probability level (hydrogen atoms omitted for clarity). Fe orange, C black, N blue, O red.
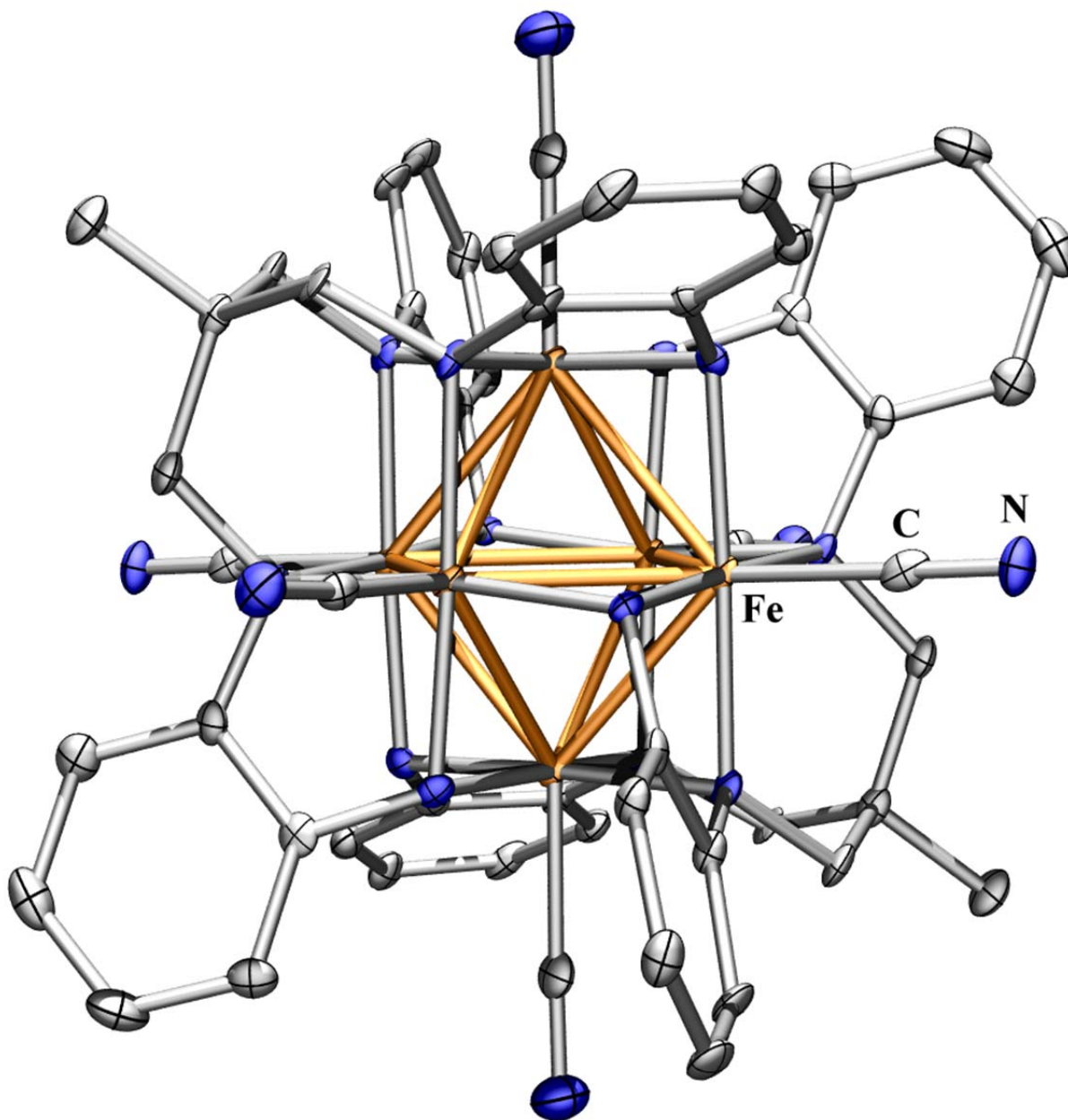
Figure S5. Solid state molecular structure of $[(^HL)_2Fe_6(CN)_6]^{3-}$, anion of **7**. Thermal ellipsoids set at 50% probability level (hydrogen atoms omitted for clarity). Fe orange, C black, N blue.

Figure S6. Solid state molecular structure of [(^{H}L)$_2$Fe$_6$(CN)$_6$]$^{2-}$, anion of **8**. Thermal ellipsoids set at 50% probability level (hydrogen atoms omitted for clarity). Fe orange, C black, N blue.

Figure S7. Solid state molecular structure of $[(^{H}L)_2Fe_6(CN)_6]^-$, anion of **9**. Thermal ellipsoids set at 50% probability level (hydrogen atoms omitted for clarity). Fe orange, C black, N blue.
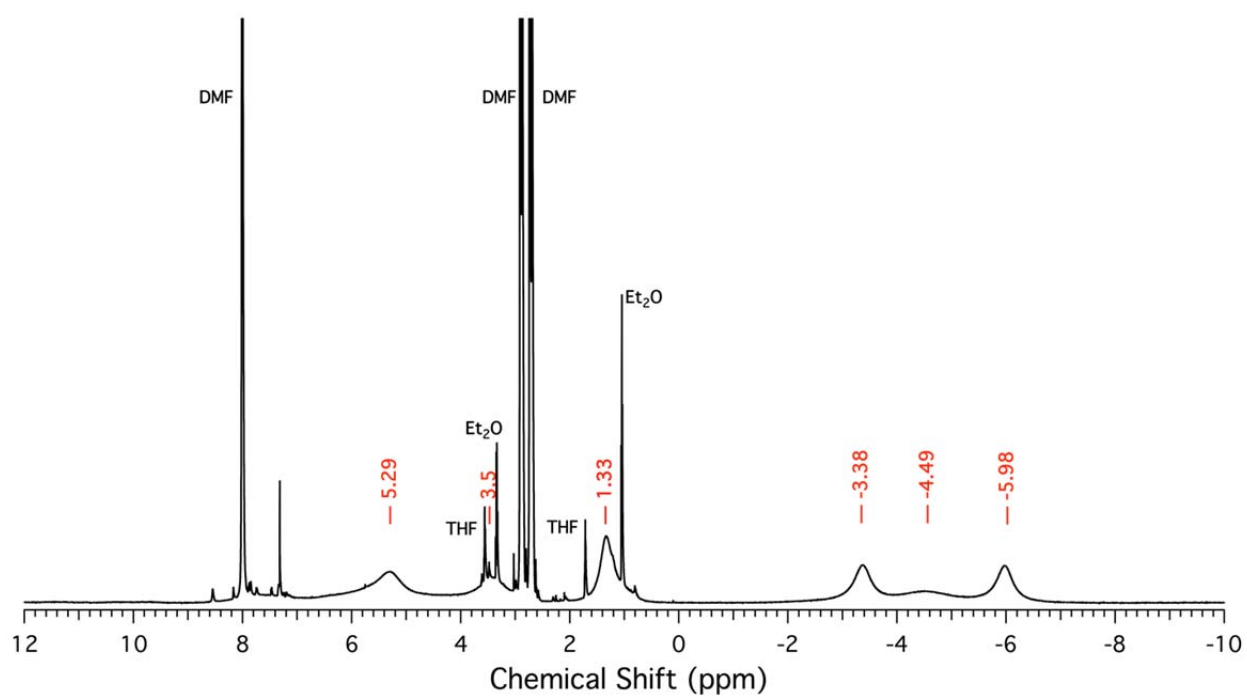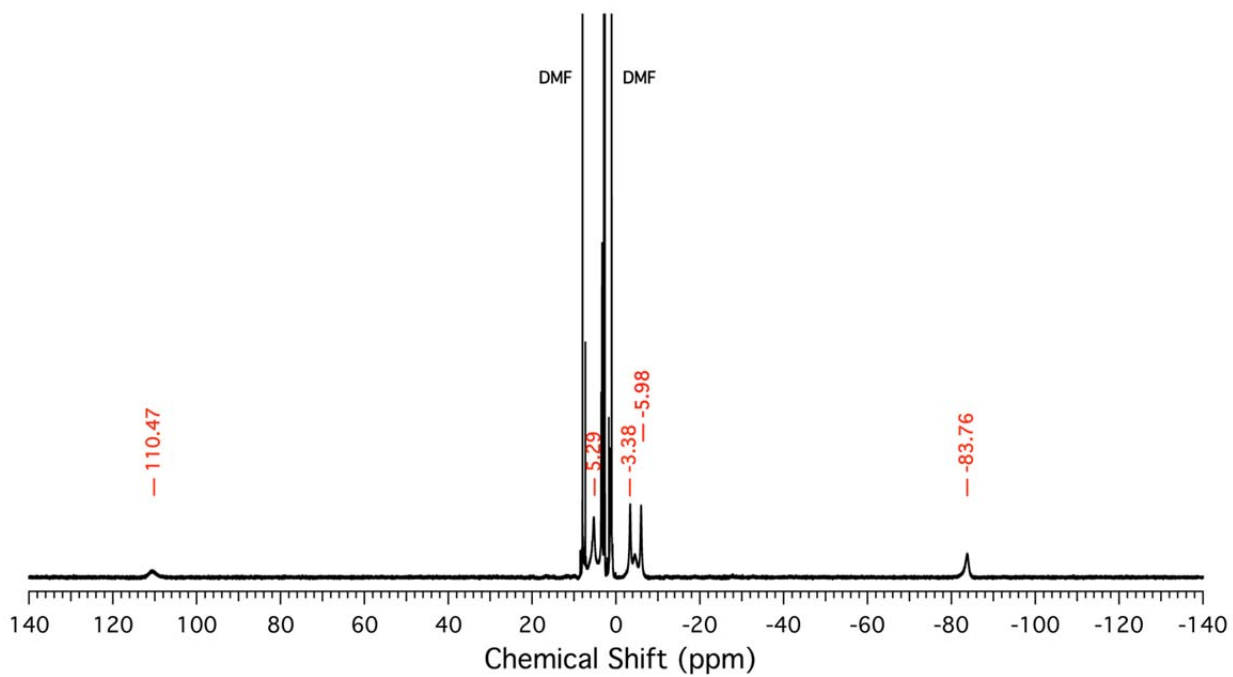
Figure S8. ¹H NMR spectrum of [(^HL)₂Fe₆(DMF)₄][PF₆]₂, **4**. Taken in DMF-*d*₇ and referenced to residual solvent peaks (1H, 8.01; 3H, 2.91; 3H, 2.74 ppm).
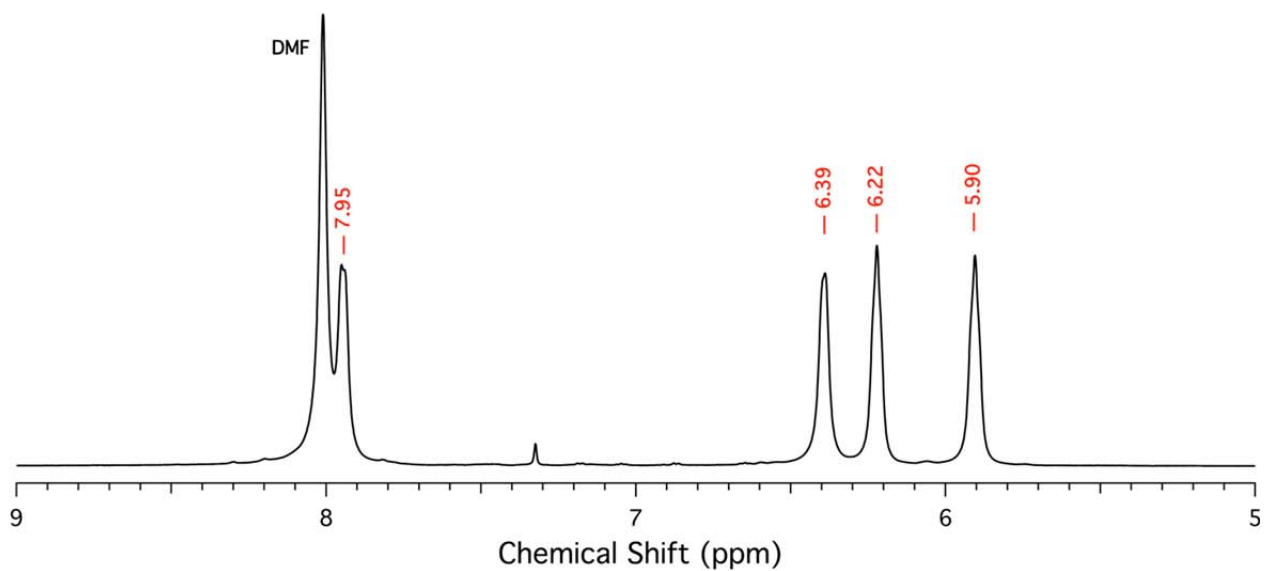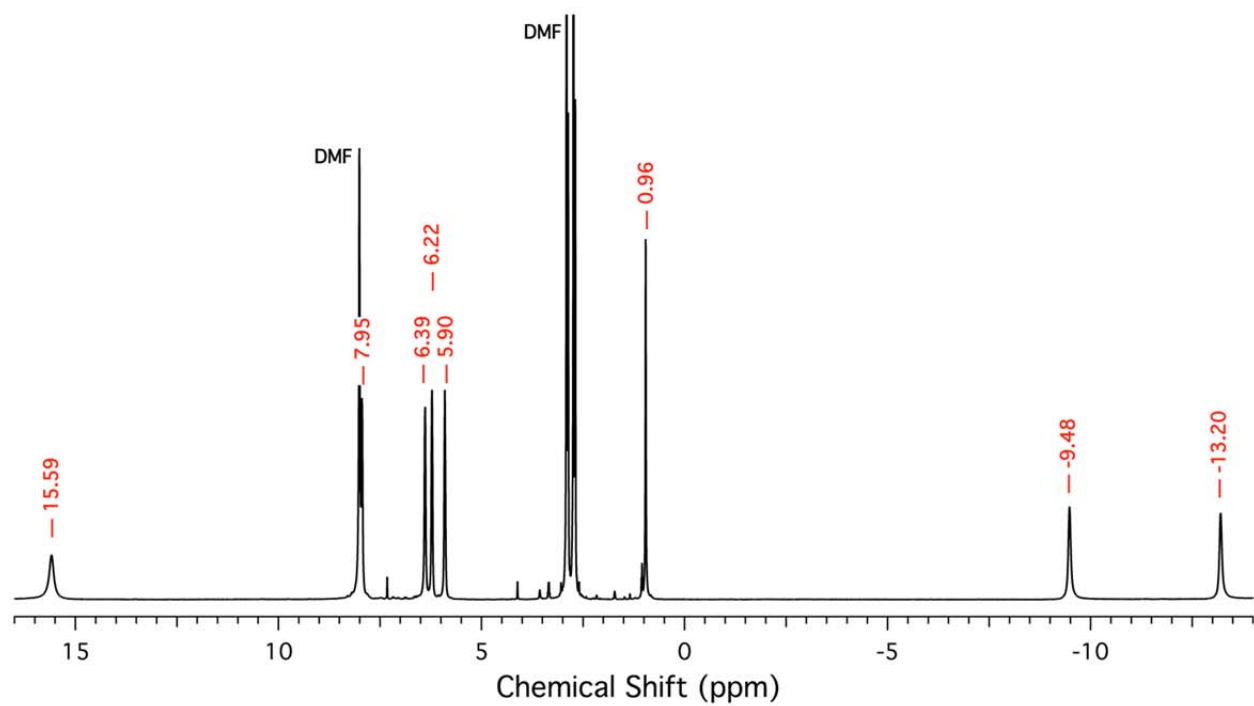
Figure S9. ^{1}H NMR spectrum of $[(^HL)_2Fe_6(DMF)_6][PF_6]_3$, **5**. Taken in DMF-$d_7$ and referenced to residual solvent peaks (1H, 8.01; 3H, 2.91; 3H, 2.74 ppm).
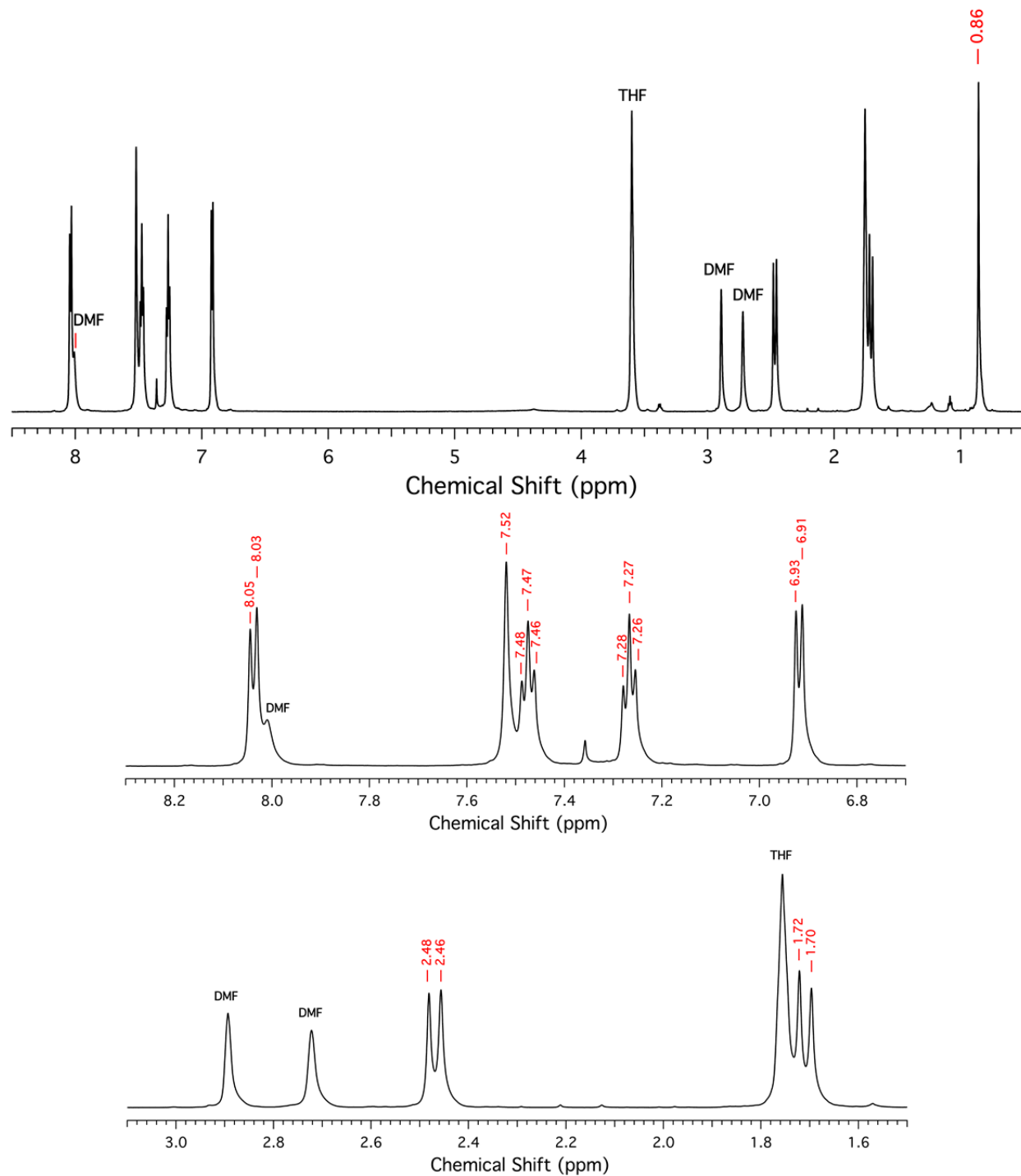
Figure S10. ¹H NMR spectrum of [(ᴴL)₂Fe₆(DMF)₆][BF₄]₄, **6**. δ (ppm): 8.05-8.03 (aryl C–*H*, 6H), 7.52 (aryl N–*H*, 6H), 7.47 (aryl C–*H*, 6H), 7.27 (aryl C–*H*, 6H), 6.93-6.91 (aryl C–*H*, 6H), 2.48-2.46 and 1.72-1.70 (C–C*H*₂–aryl, 12H), 0.86 (CC*H*₃, 6H). Taken in DMF-*d*₇ and referenced to residual solvent peaks (1H, 8.01; 3H, 2.91; 3H, 2.74 ppm).
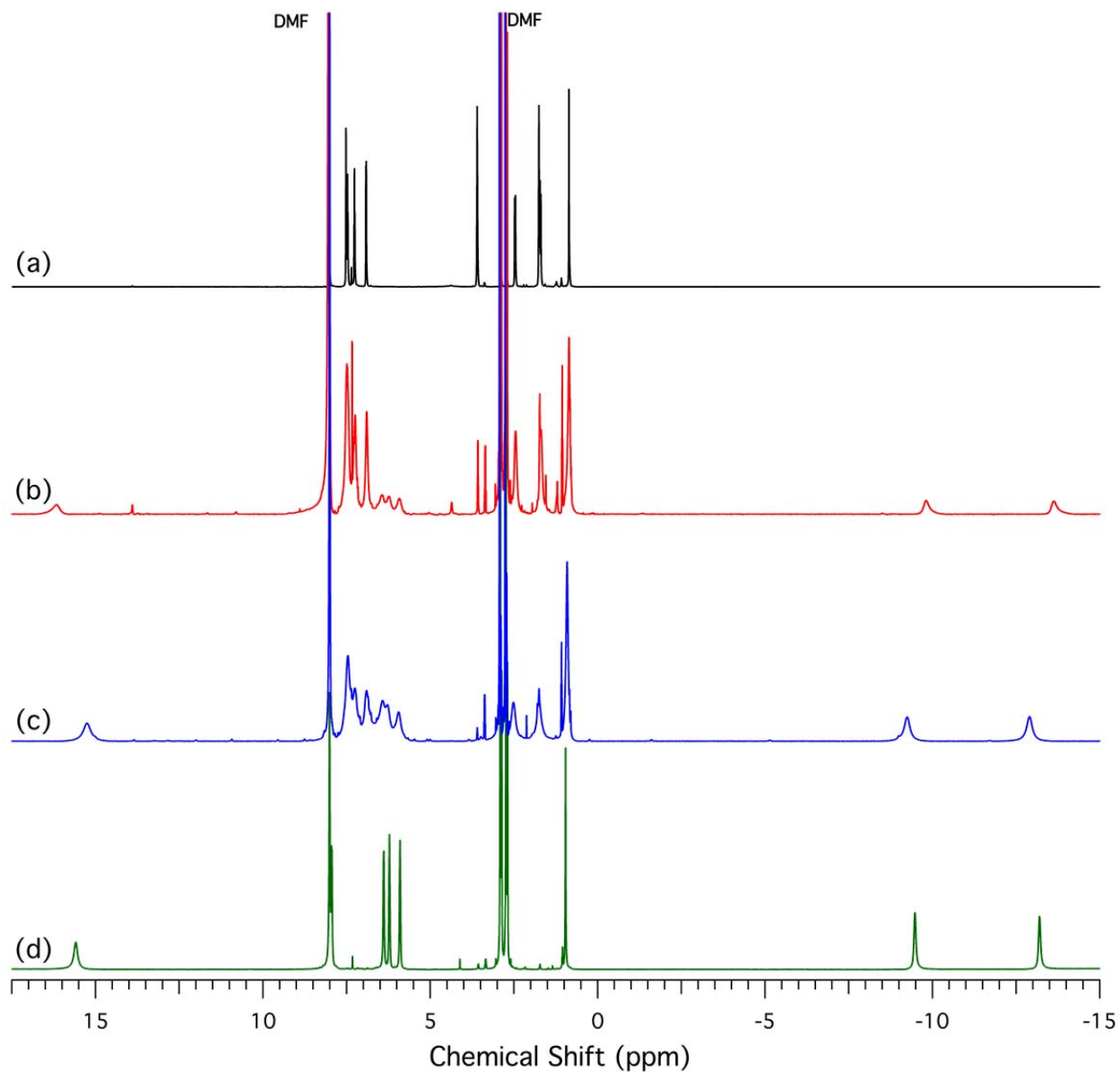
Figure S11. ^{1}H NMR spectrum of $[(^HL)_2Fe_6(DMF)_6][BF_4]_4$ (**6**) at different time intervals. (a) Oxidation *in situ* (same as in Figure S10), worked up **6** standing as a solid at room temperature for (b) 5h, and (c) 6 days, and (d) $[(^HL)_2Fe_6(DMF)_6][PF_6]_3$ (**5**). Taken in DMF-d_7 and referenced to residual solvent peaks (1H, 8.01; 3H, 2.91; 3H, 2.74 ppm)
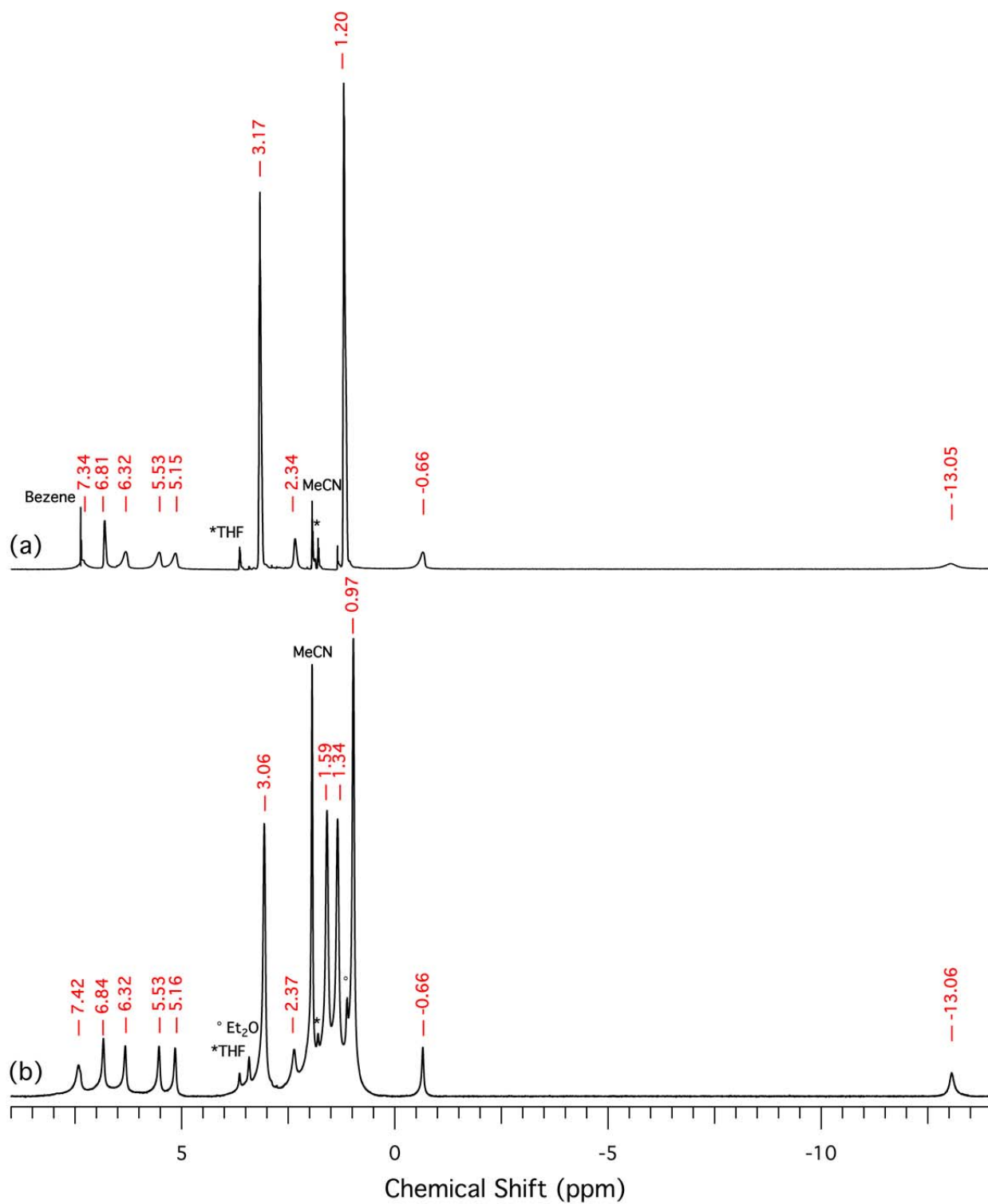
Figure S12. ^1H NMR spectrum of $[R_4N]_3[(^HL)_2Fe_6(CN)_6]$ for R = (a) Et and (b) Bu (**7**). Taken in MeCN-d_3 and referenced to residual solvent peaks (1.94 ppm).
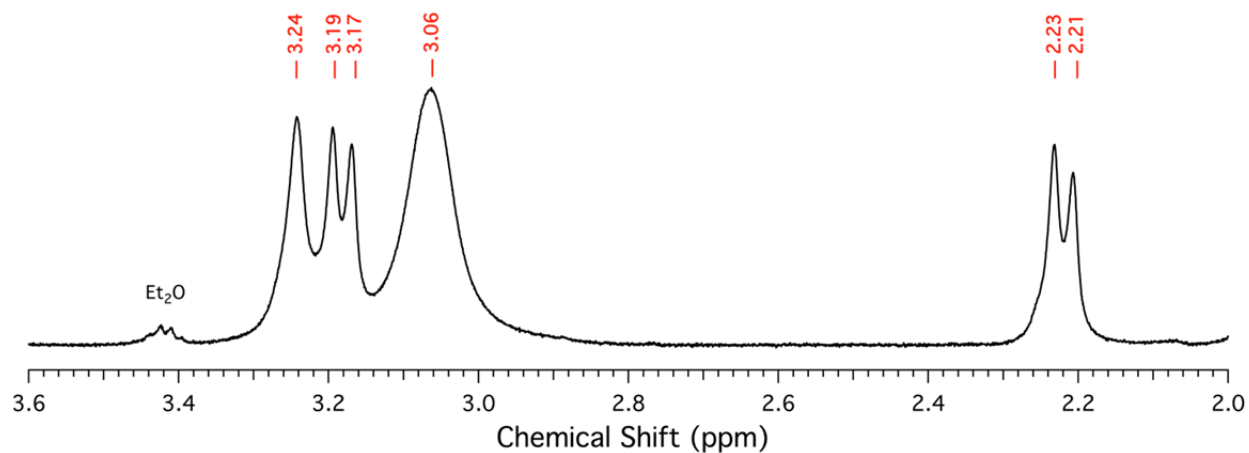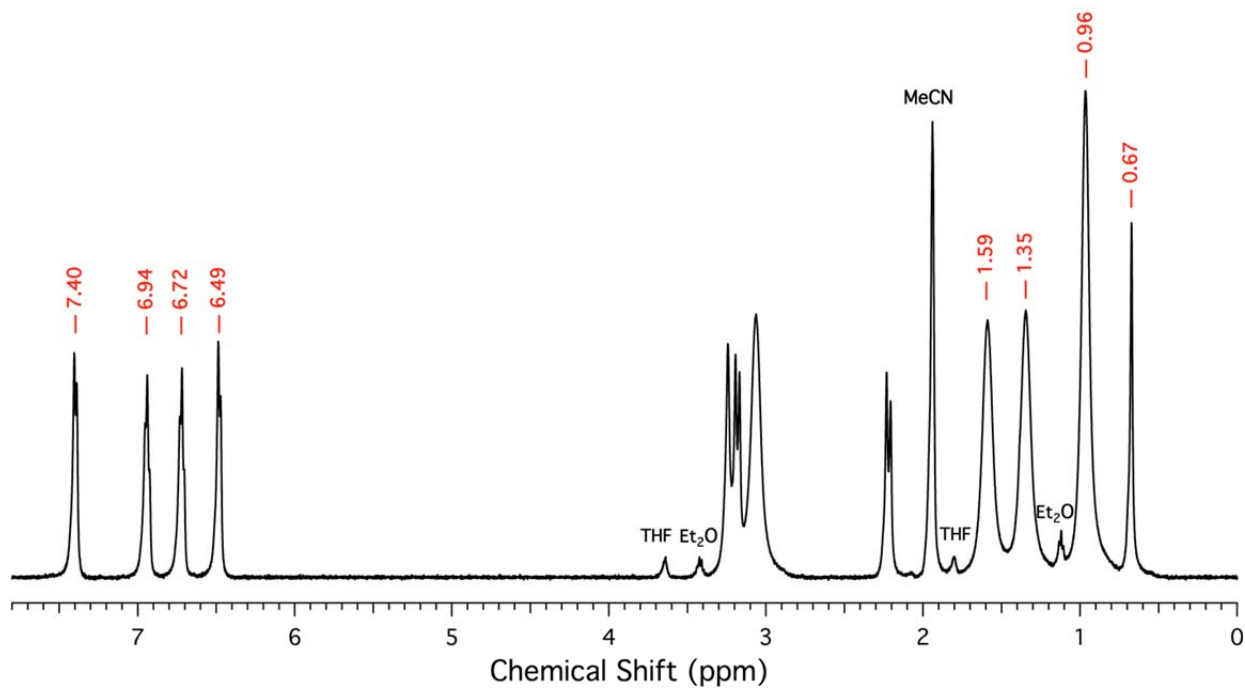
Figure S13. ^{1}H NMR spectrum of [Bu$_4$N]$_2$[(^{H}L)$_2$Fe$_6$(CN)$_6$], **8**. δ (ppm): 7.40 (aryl C–*H*, 6H), 6.94 (aryl C–*H*, 6H), 6.72 (aryl C–*H*, 6H), 6.49 (aryl C–*H*, 6H), 3.24 (aryl N–*H*, 6H), 3.19-3.17 and 2.23-2.21 (C–C*H*$_2$–aryl, 12H), 3.06 ([N(C*H*$_2$CH$_2$CH$_2$CH$_3$)$_4$], 8H), 1.59 ([N(CH$_2$C*H*$_2$CH$_2$CH$_3$)$_4$], 8H), 1.35 ([N(CH$_2$CH$_2$C*H*$_2$CH$_3$)$_4$], 8H), 0.96 ([N(CH$_2$CH$_2$CH$_2$C*H*$_3$)$_4$], 12H), 0.67 (CC*H*$_3$, 6H). Taken in MeCN-*d*$_3$ and referenced to residual solvent peaks (1.94 ppm).
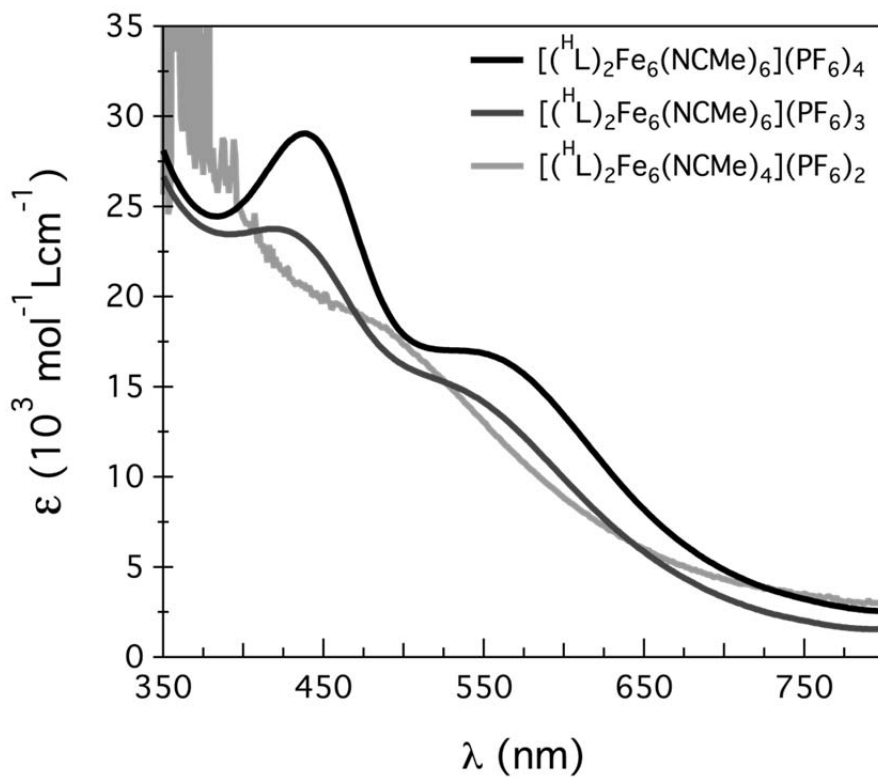
	λ_{max} (nm)	ε_{max} (mol^{-1}Lcm^{-1})
1	~490	~18000
2	417	24580
	~550	~15000
3	439	29800
	~570	~17000

Figure S14. UV/Vis spectra of [(^{H}L)$_2$Fe$_6$(NCMe)$_4$][PF$_6$]$_2$, **1**; [(^{H}L)$_2$Fe$_6$(NCMe)$_6$][PF$_6$]$_3$, **2**; and [(^{H}L)$_2$Fe$_6$(NCMe)$_6$][PF$_6$]$_4$, **3**. Taken in MeCN.
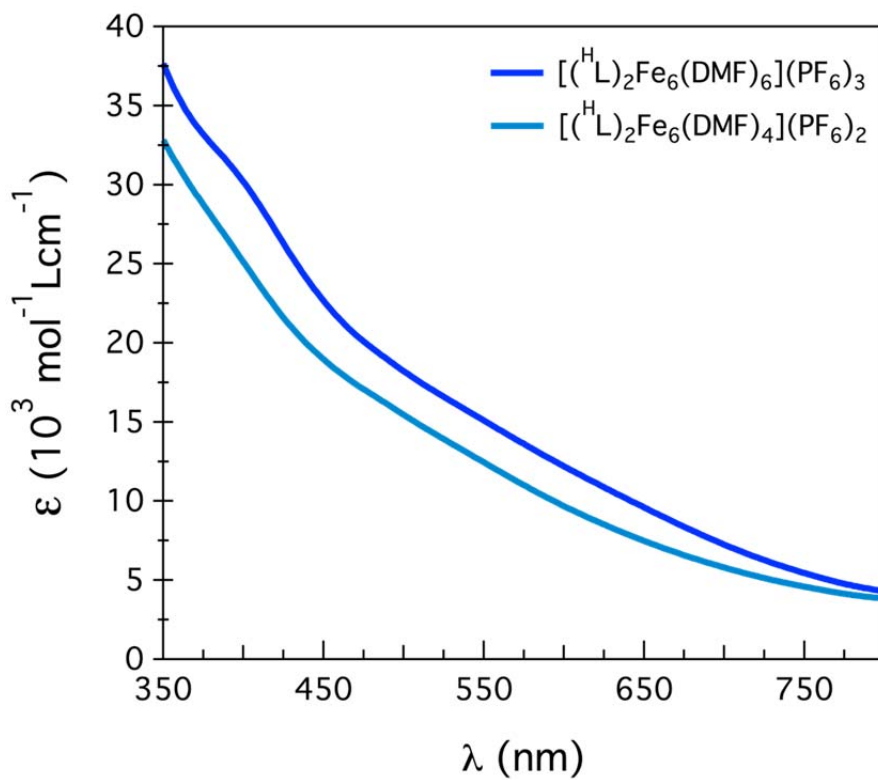
	λ_{max} (nm)	ε_{max} (mol^{-1}Lcm^{-1})
5	~400	~30000

Figure S15. UV/Vis spectra of [(^{H}L)$_2$Fe$_6$(DMF)$_4$][PF$_6$]$_2$, **4**; and [(^{H}L)$_2$Fe$_6$(DMF)$_6$][PF$_6$]$_3$, **5**. Taken in DMF.
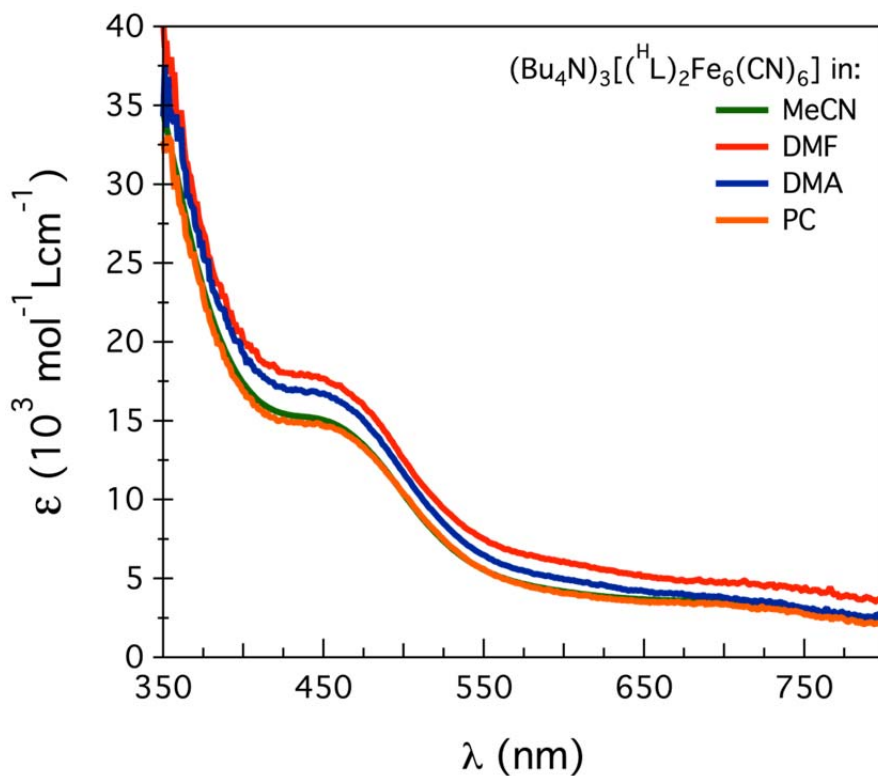
	Solvent	λ_{max} (nm)	ε_{max} (mol^{-1}Lcm^{-1})
	MeCN	~450	~15000
7	DMF	~450	~18000
	DMA	~450	~17000
	PC	~450	~15000

Figure S16. UV/Vis spectra of [Bu$_4$N]$_3$[(^{H}L)$_2$Fe$_6$(CN)$_6$], **7**. Taken in four different solvents: MeCN, DMF, DMA, and propylene carbonate (PC). A very broad absorption band is observed at ~700 nm in all solvents that was not analyzed in further detail.
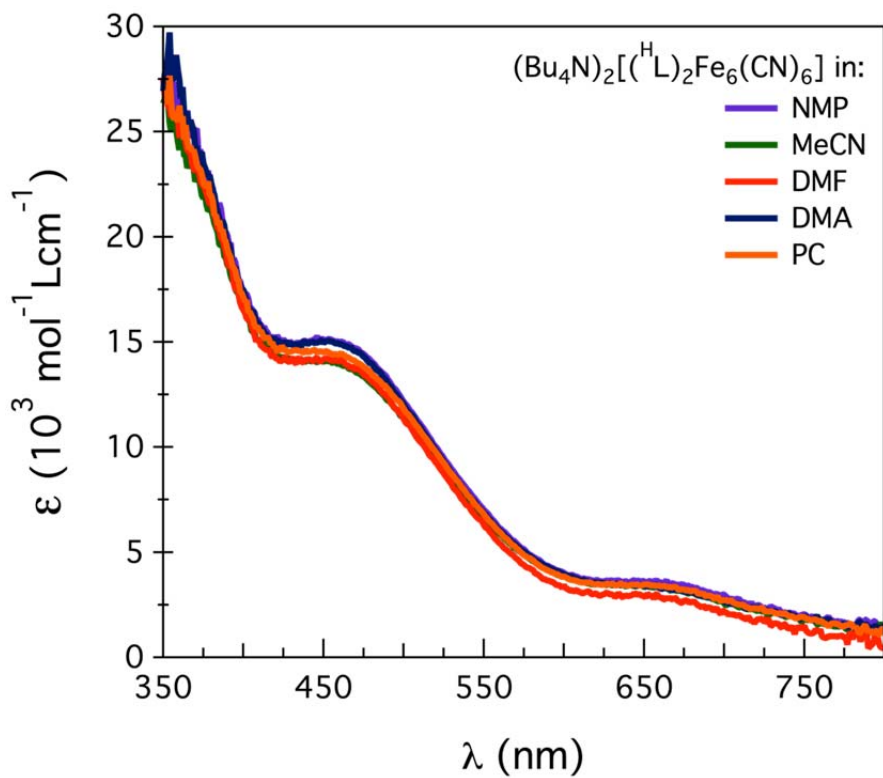
|	Solvent	λ_{max} (nm)	ε_{max} (mol^{-1}Lcm^{-1})
	NMP	~460	~15000
	MeCN	~460	~14000
8	DMF	~460	~14000
	DMA	~460	~15000
	PC	~460	~14500

Figure S17. UV/Vis spectra of [Bu$_4$N]$_2$[(^{H}L)$_2$Fe$_6$(CN)$_6$], **8**. Taken in five different solvents: *N*-Methyl-2-pyrrolidone (NMP), MeCN, DMF, DMA, and PC. A very broad absorption band is observed at ~670 nm in all solvents that was not analyzed in further detail.
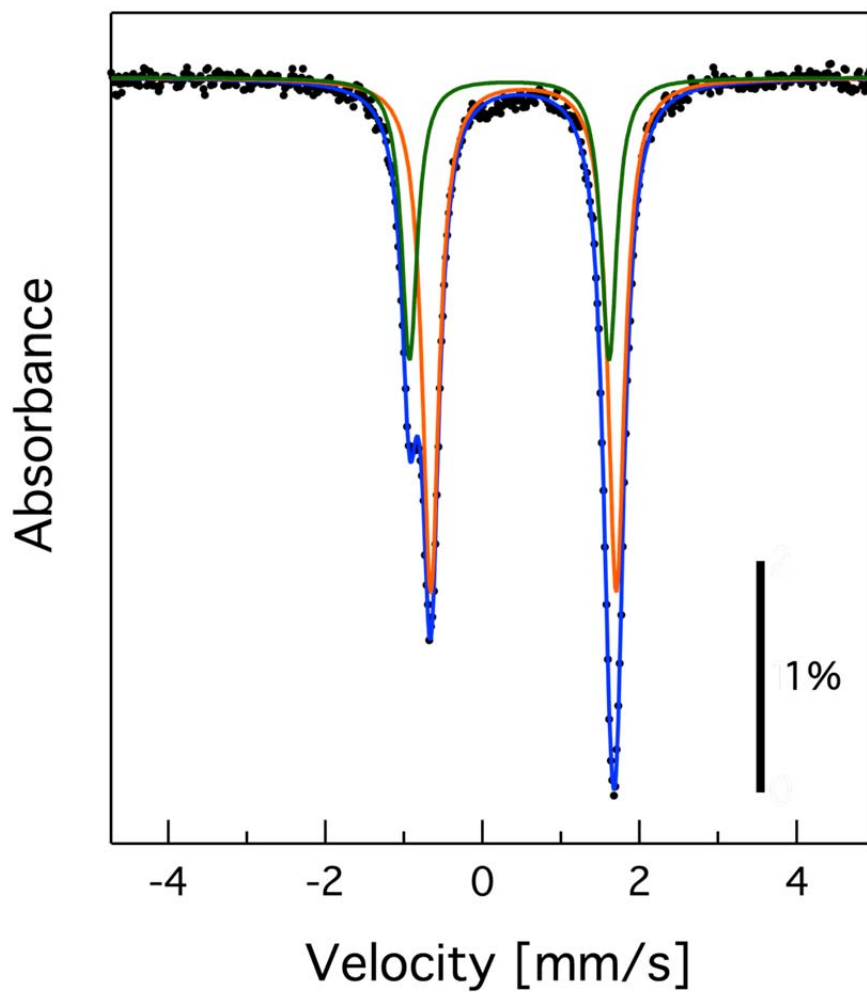
Figure S18. Zero-field ^{57}Fe Mössbauer spectrum of [(^{H}L)$_2$Fe$_6$(DMF)$_4$][PF$_6$]$_2$, **4**. δ, $|\Delta E_Q|$ (mm/s):
(90 K) component 1 (orange line): 0.52, 2.36, 66% ($\gamma = 0.26$ mm/s); component 2 (green line):
0.34, 2.54, 34% ($\gamma = 0.24$ mm/s).
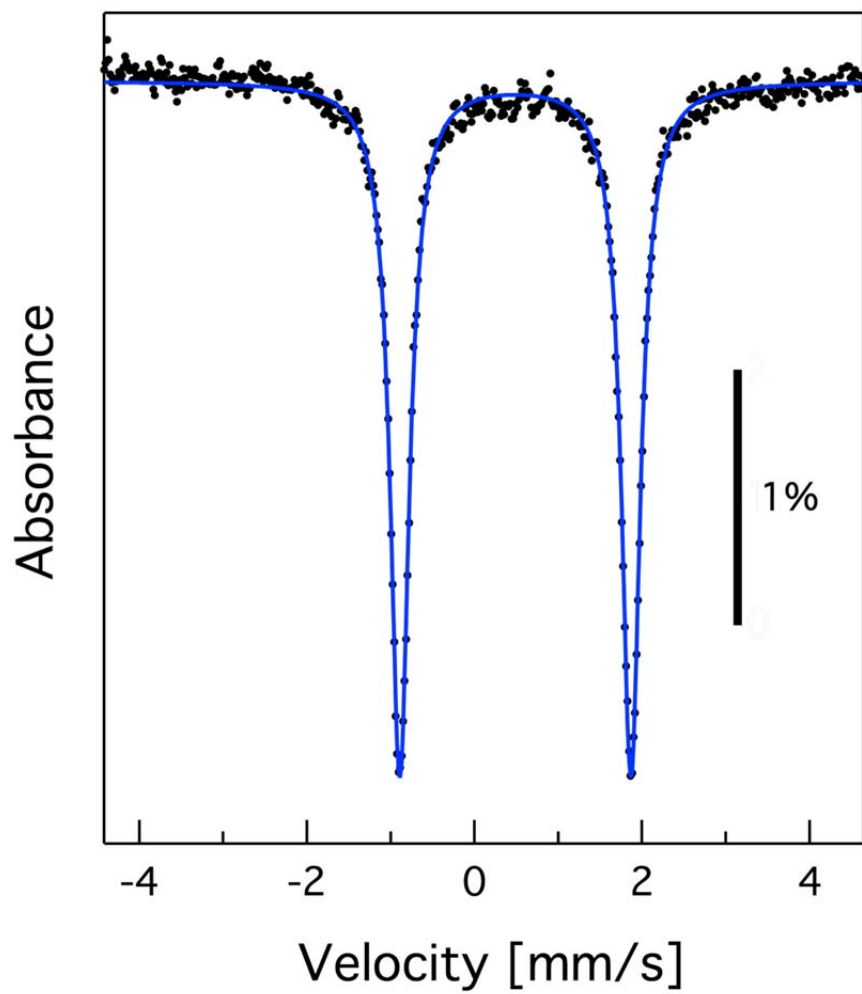
Figure S19. Zero-field ^{57}Fe Mössbauer spectrum of $[(^{H}L)_2Fe_6(DMF)_6][PF_6]_3$, **5**. δ, $|\Delta E_Q|$ (mm/s): (90 K) 0.49, 2.76 (γ = 0.28 mm/s).
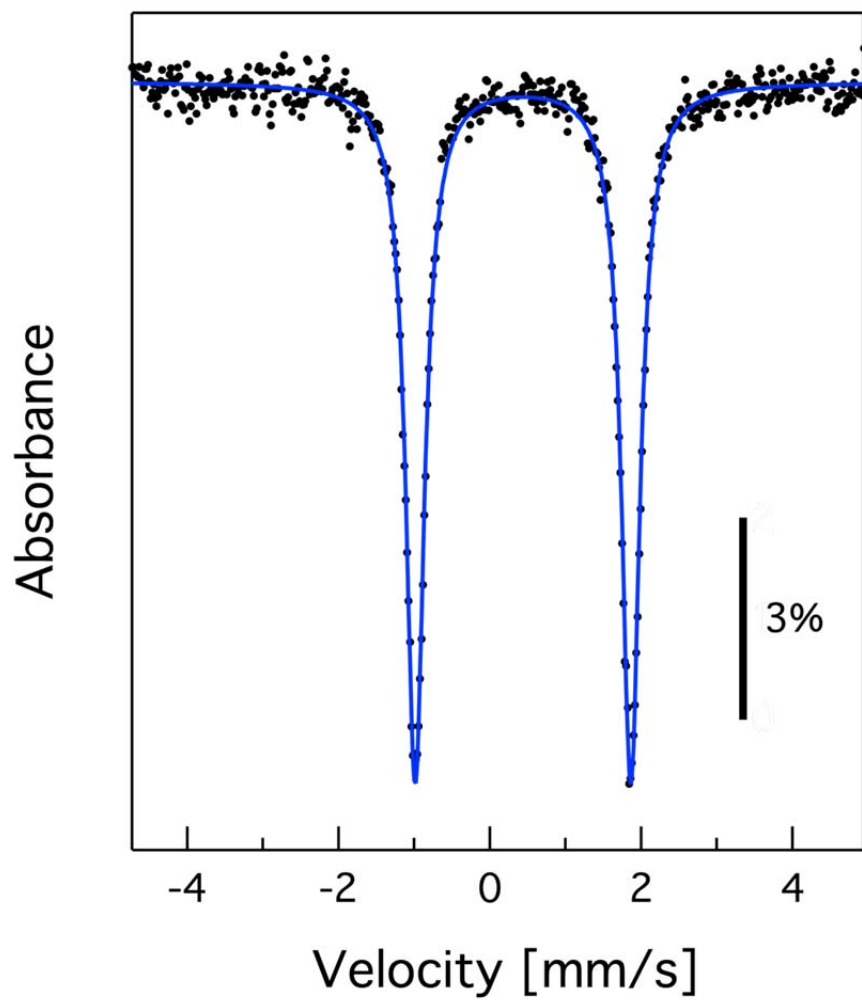
Figure S20. Zero-field ^{57}Fe Mössbauer spectrum of [(^{H}L)$_2$Fe$_6$(DMF)$_6$][BF$_4$]$_4$, **6**. δ, $|\Delta E_Q|$ (mm/s): (90 K) 0.44, 2.85 (γ = 0.30 mm/s).
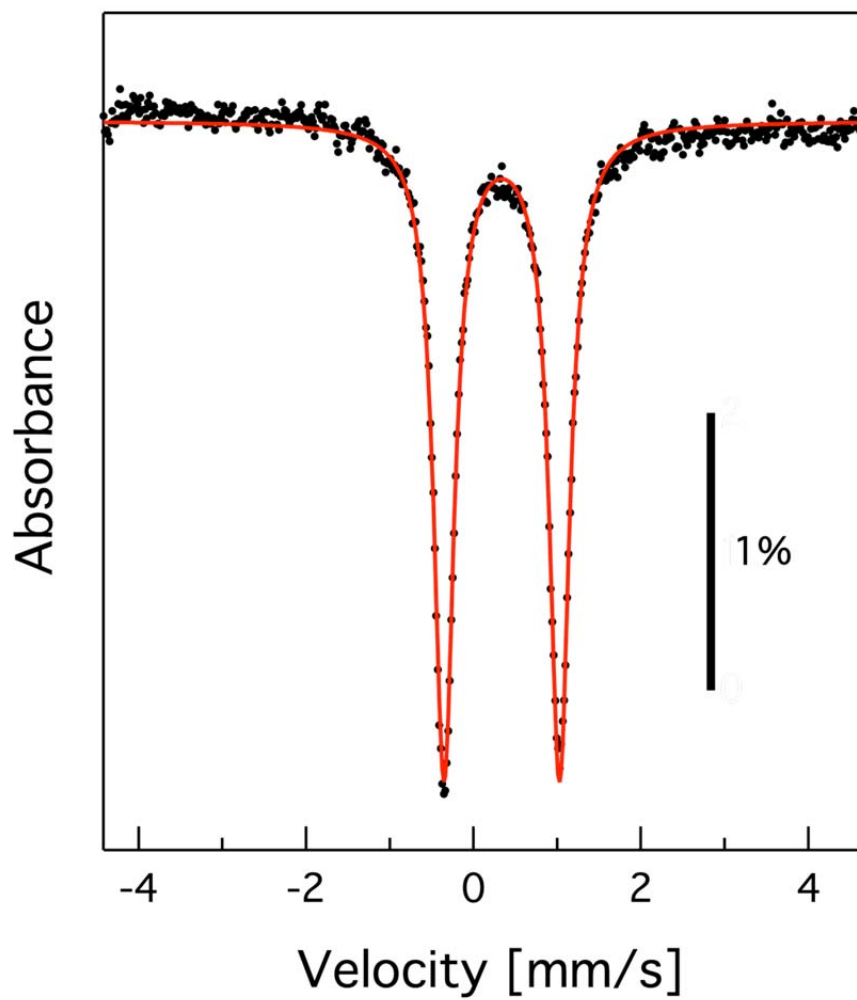
Figure S21. Zero-field ^{57}Fe Mössbauer spectrum of [Bu$_4$N]$_3$[(^{H}L)$_2$Fe$_6$(CN)$_6$], **7**. δ, |ΔE_Q| (mm/s): (90 K) 0.34, 1.38 (γ = 0.30 mm/s).
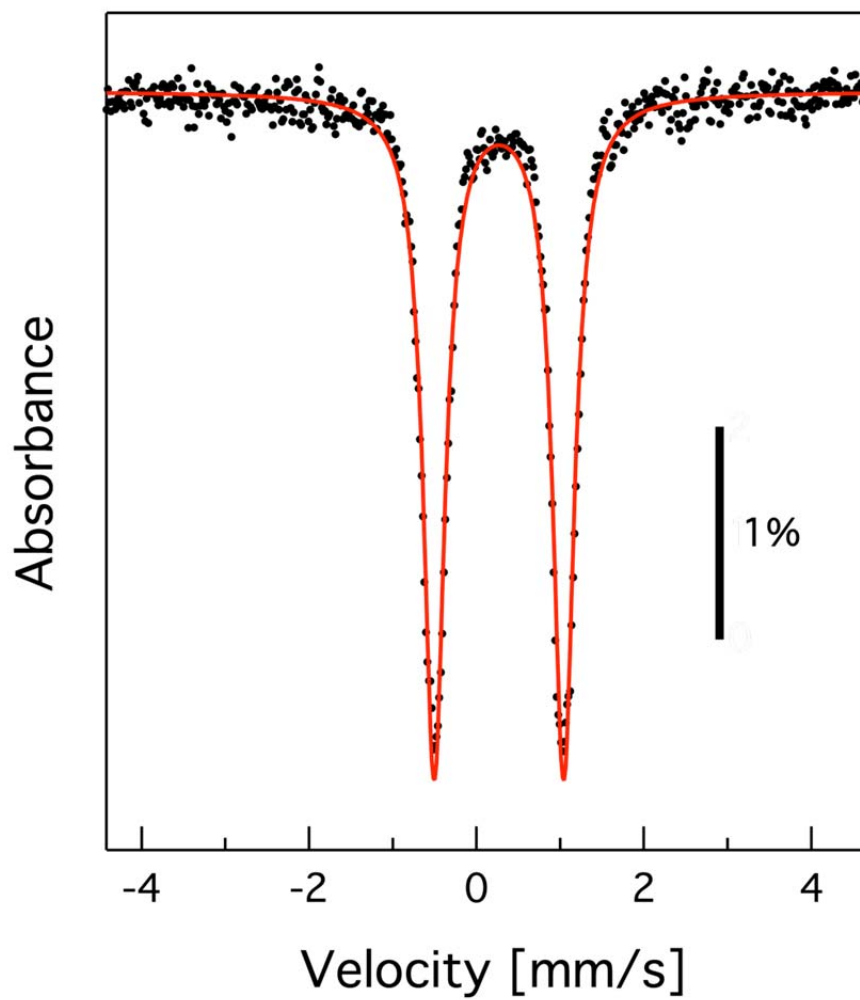
Figure S22. Zero-field ^{57}Fe Mössbauer spectrum of [Bu$_4$N]$_2$[(^{H}L)$_2$Fe$_6$(CN)$_6$], **8**. δ, |ΔE_Q| (mm/s): (90 K) 0.27, 1.55 (γ = 0.32 mm/s).
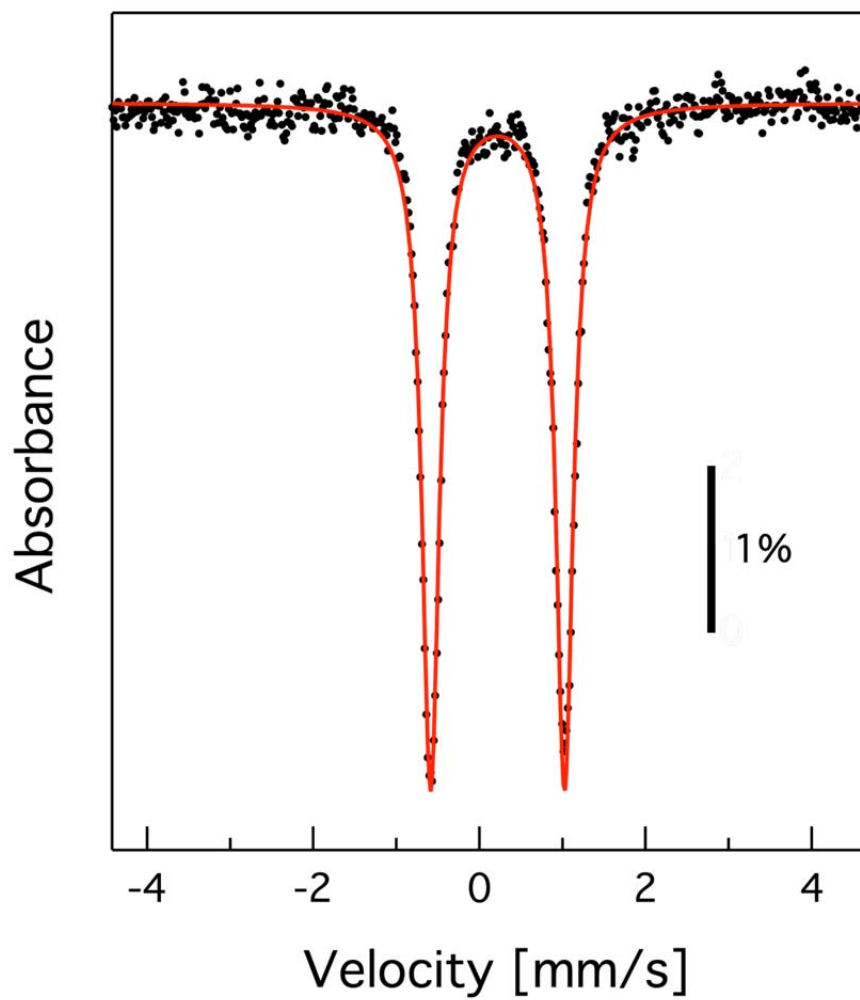
Figure S23. Zero-field ^{57}Fe Mössbauer spectrum of [Bu$_4$N][(^{H}L)$_2$Fe$_6$(CN)$_6$], **9**. δ, |ΔE_Q| (mm/s): (90 K) 0.22, 1.61 (γ = 0.26 mm/s).
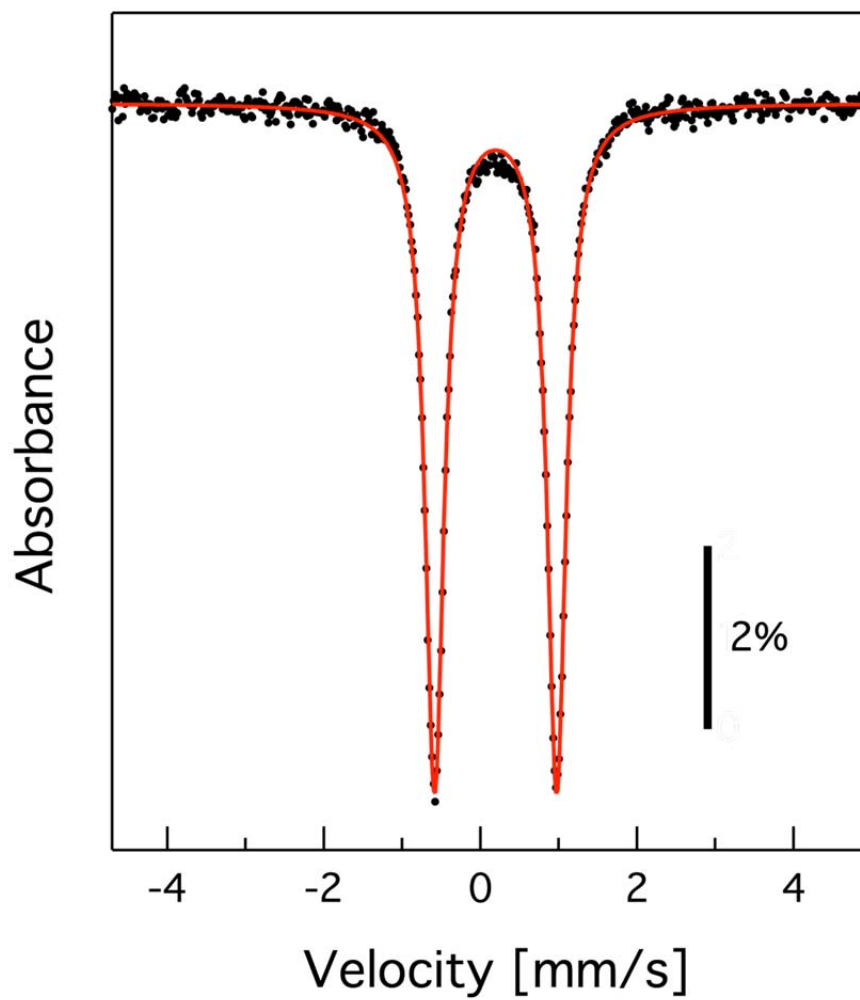
Figure S24. Zero-field ^{57}Fe Mössbauer spectrum of $(^{H}L)_2Fe_6(CN)_6$, **10**. δ, $|\Delta E_Q|$ (mm/s): (90 K) 0.19, 1.56 ($\gamma = 0.30$ mm/s).
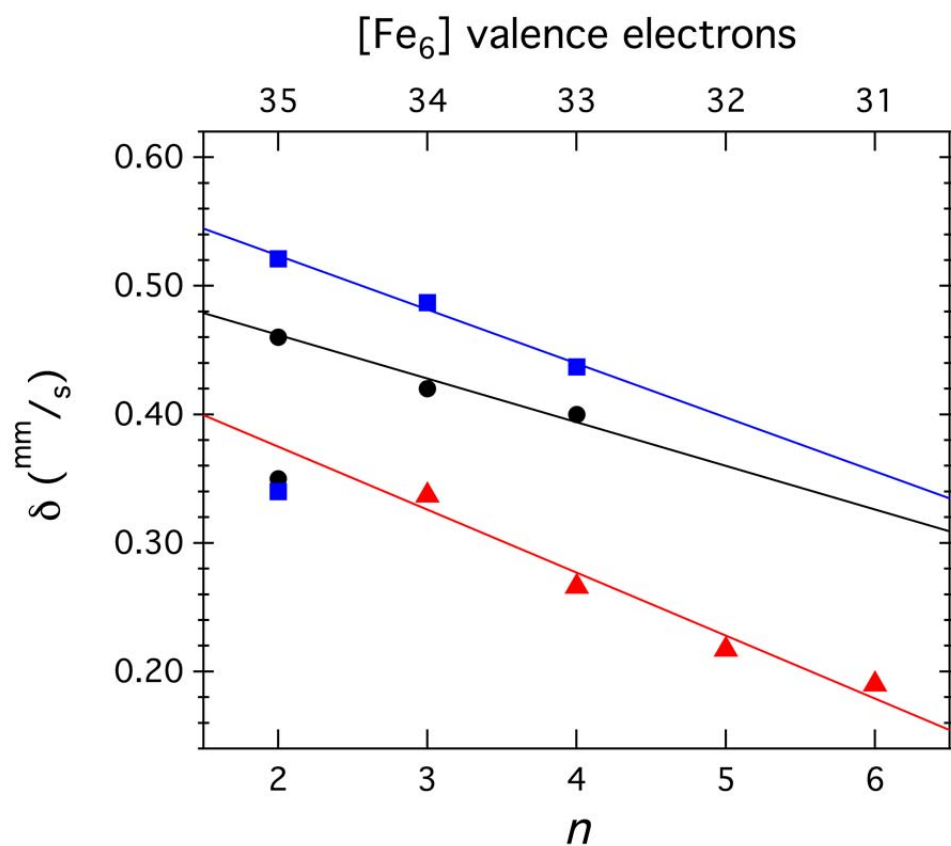
Figure S25. Isomer shift vs. oxidation level (*n*) for **1** to **3** (●), **4** to **6** (■), and **7** to **10** (▲). The isomer shift of the solvated sites were fit linearly and these are shown by the black (MeCN, **1** – **3**, *n* = 2 – 4), blue (DMF, **4** – **6**, *n* = 2 – 4), and red traces (CN, **7** – **10**, *n* = 3 – 6). The fit slopes are: –0.034(3), –0.042(4), and –0.049(6) mm/s per e^- for the MeCN, DMF, and CN electron transfer series, respectively.
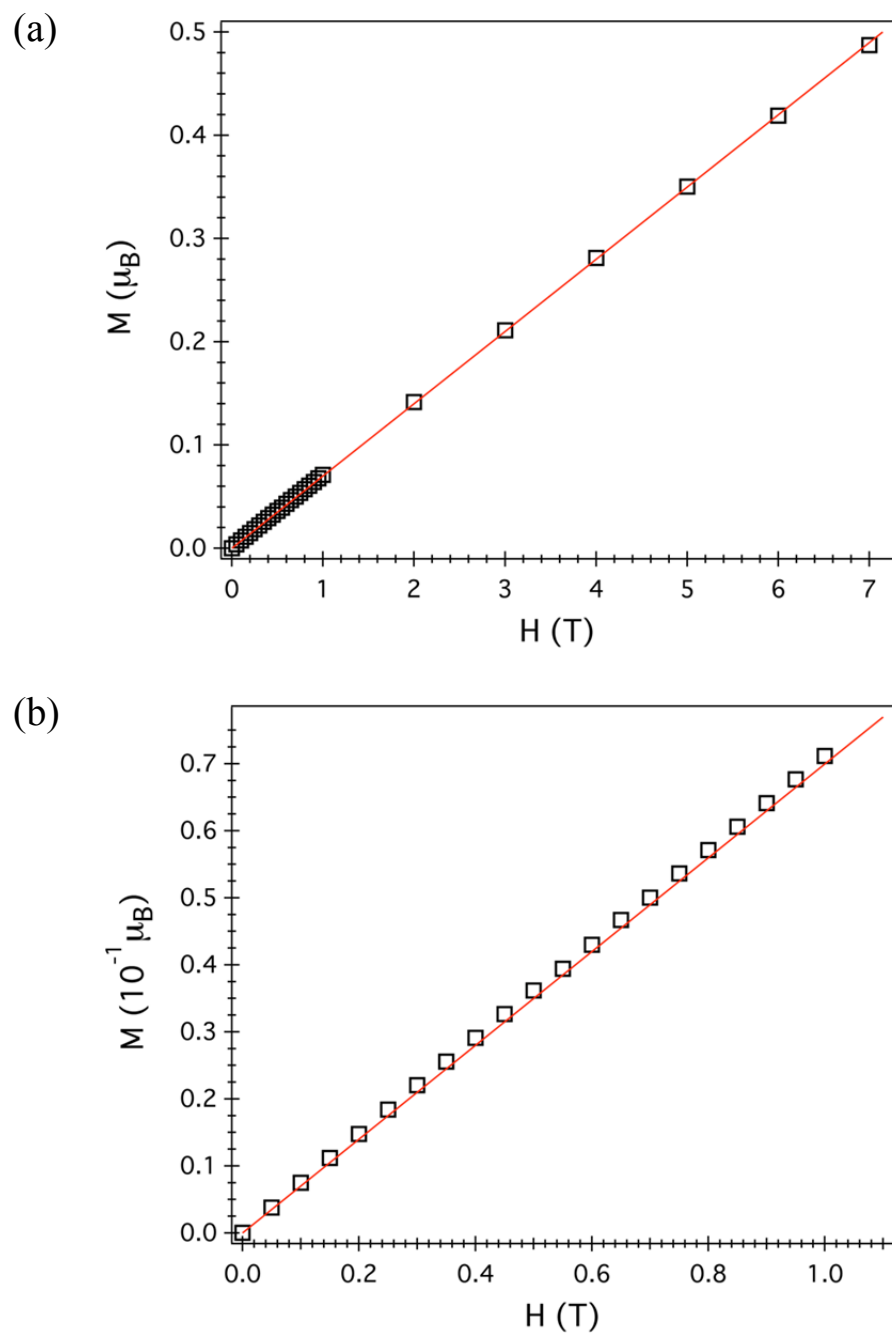
Figure S26. Magnetization data at 100 K for [(^{H}L)$_2$Fe$_6$(NCMe)$_4$][PF$_6$]$_2$, **1**. Used to check for ferromagnetic impurities. Linear fit correlation coefficient R^2 = 0.999978.

(a)

(b)
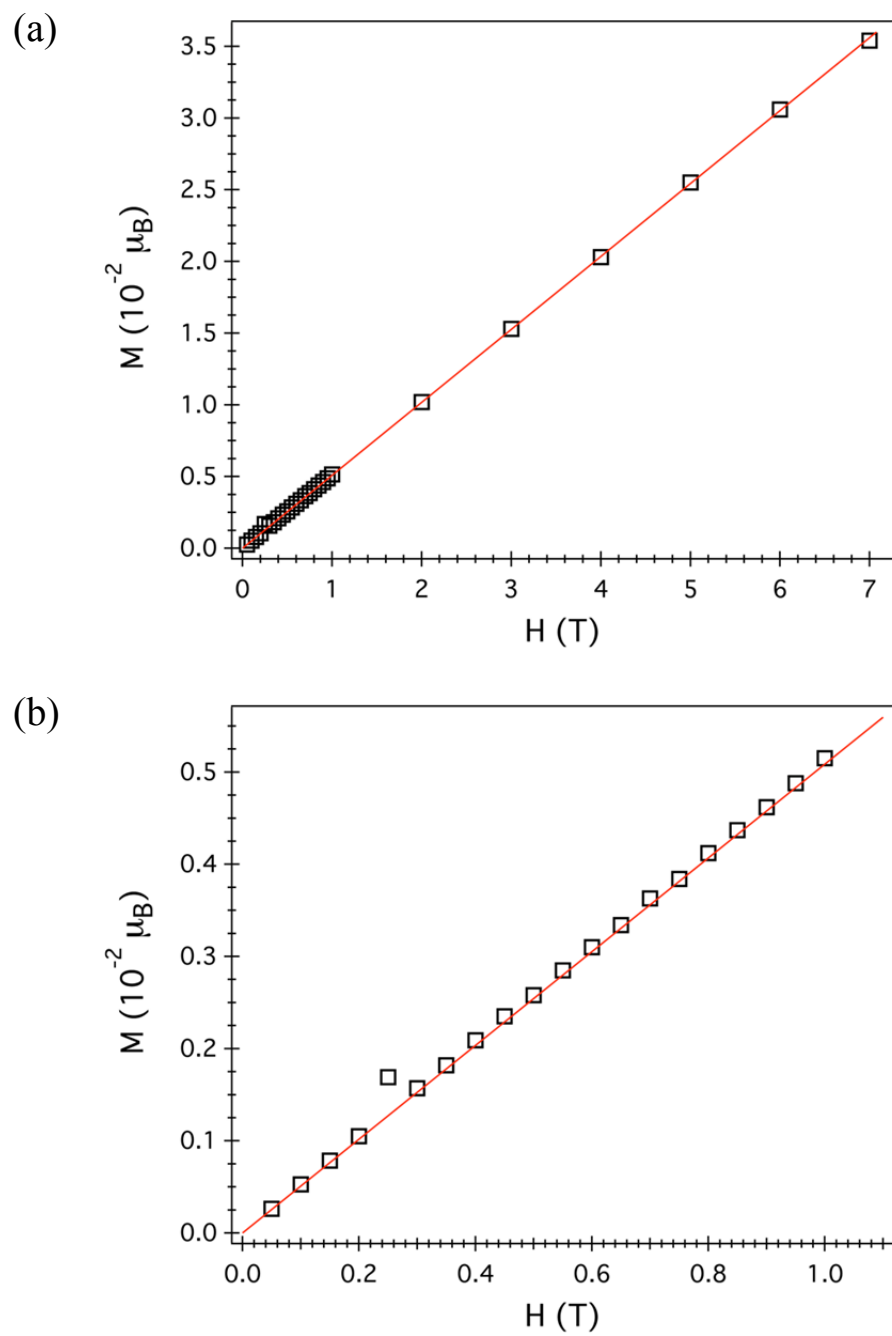
Figure S27. Magnetization data at 100 K for [(^{H}L)$_2$Fe$_6$(NCMe)$_6$][PF$_6$]$_3$, **2**. Used to check for ferromagnetic impurities. Linear fit correlation coefficient $R^2 = 0.999922$.
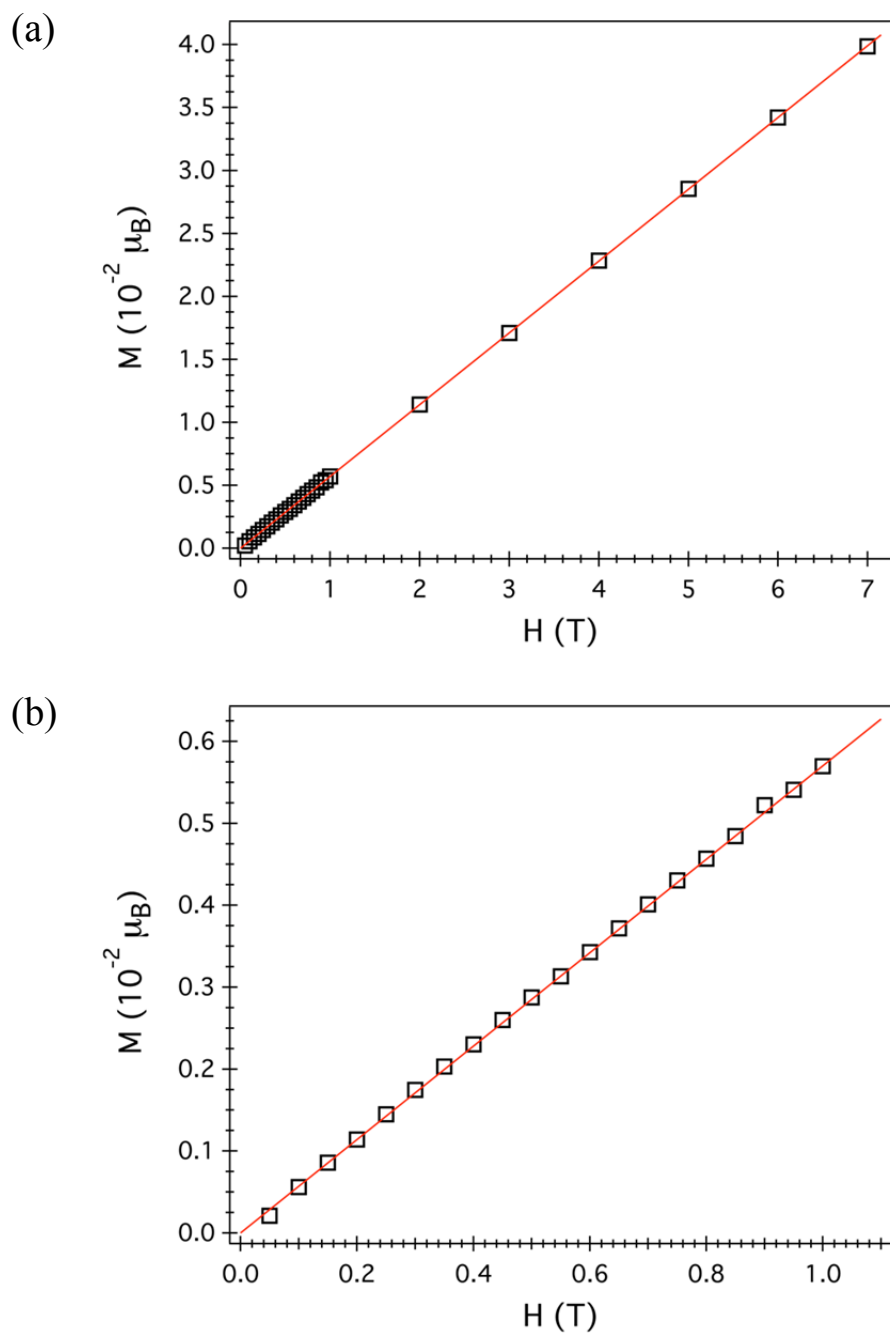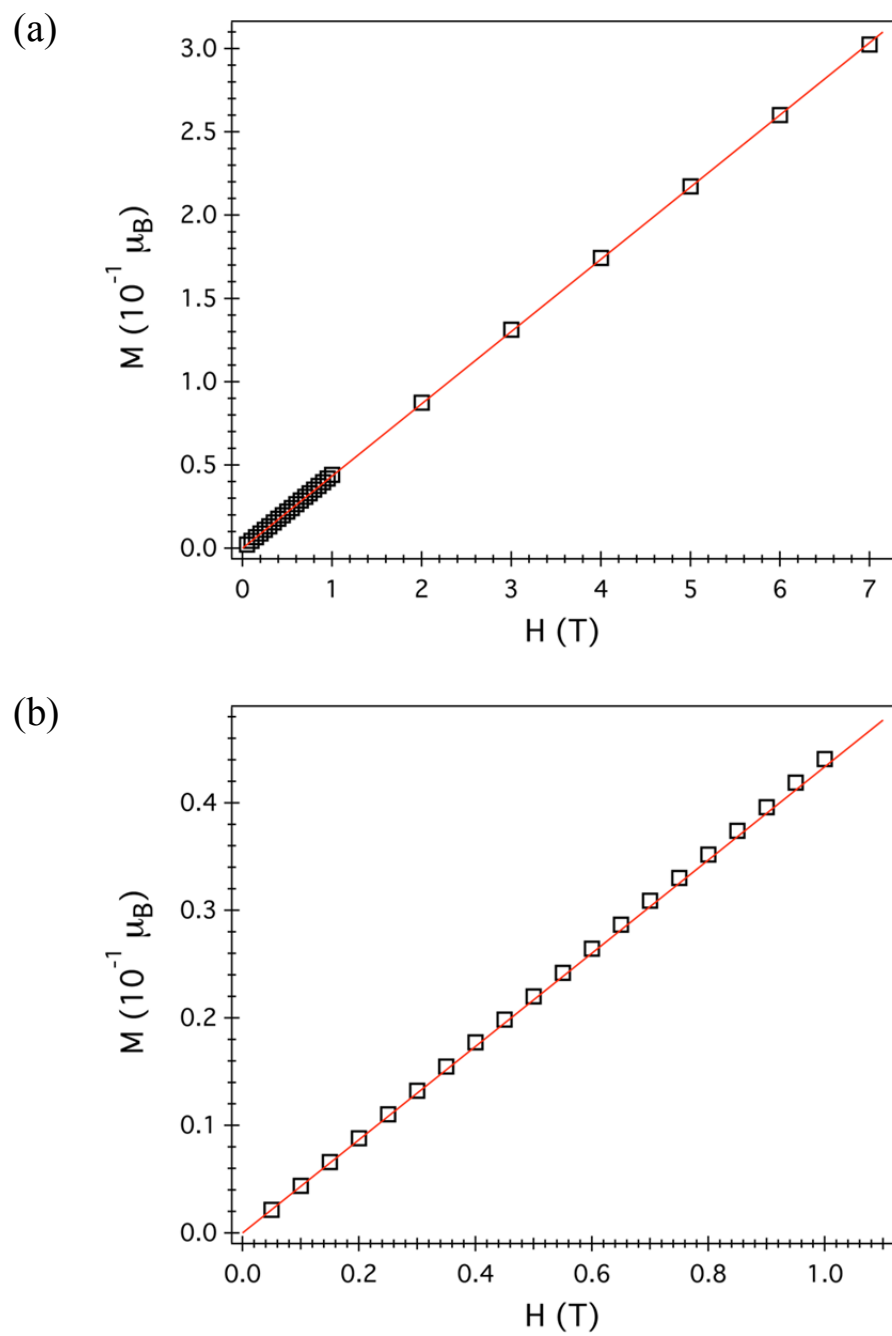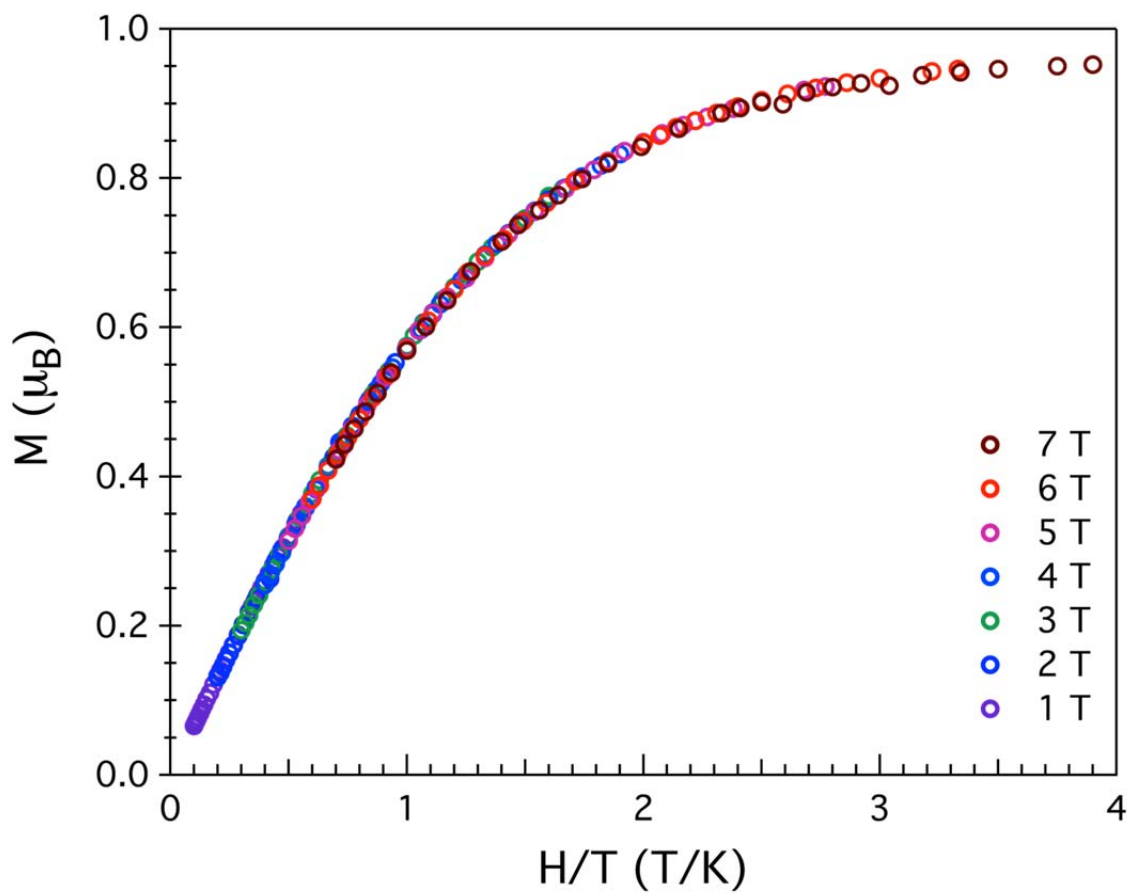
Figure S28. Magnetization data at 100 K for [(^{H}L)$_2$Fe$_6$(DMF)$_4$][PF$_6$]$_2$, **4**. Used to check for ferromagnetic impurities. Linear fit correlation coefficient R^2 = 0.999992.

(a)

(b)
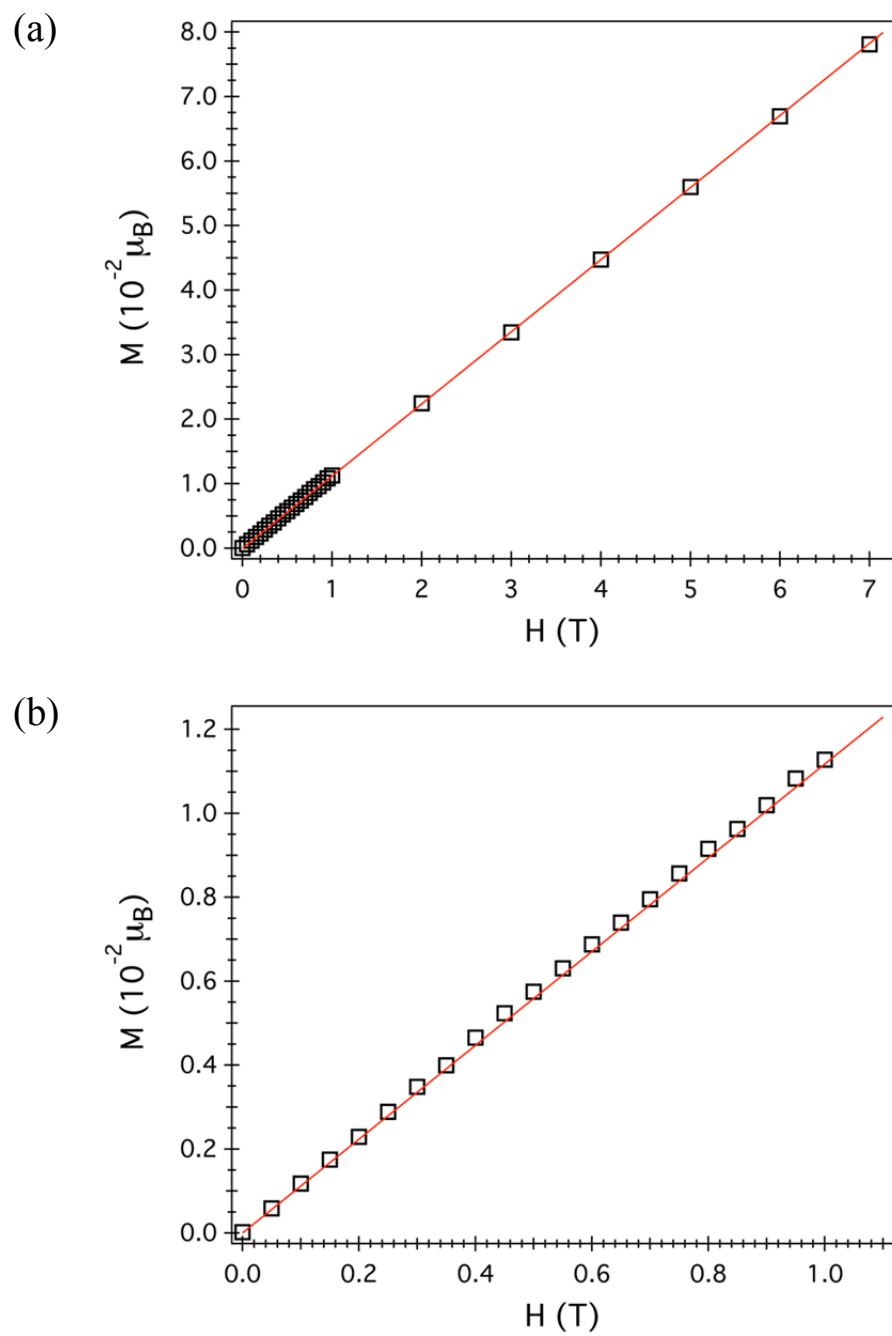
Figure S29. Magnetization data at 100 K for [(^{H}L)$_2$Fe$_6$(DMF)$_6$][PF$_6$]$_3$, **5**. Used to check for ferromagnetic impurities. Linear fit correlation coefficient $R^2 = 0.999990$.
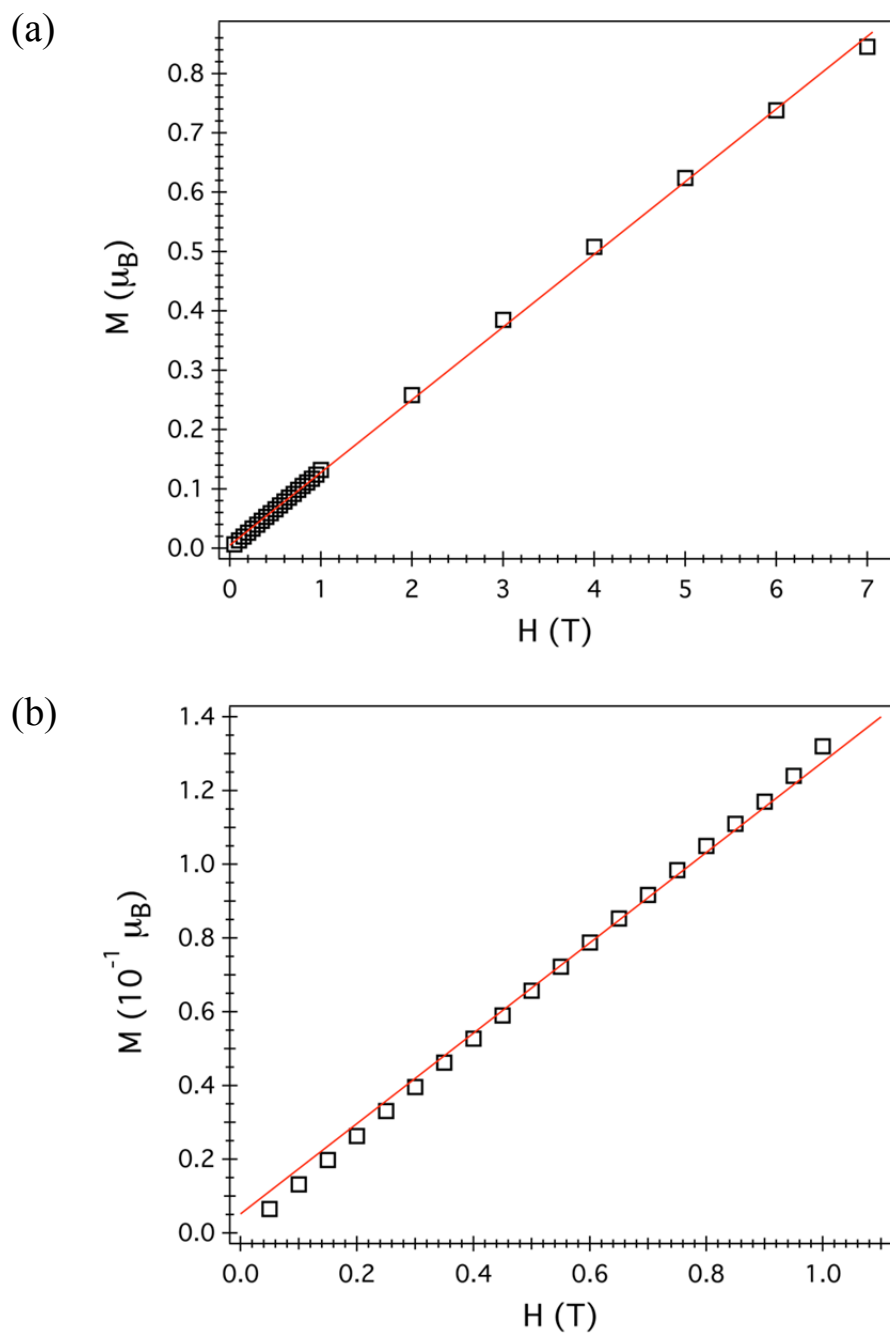
Figure S30. Magnetization data at 100 K for [Bu$_4$N]$_3$[(^{H}L)$_2$Fe$_6$(CN)$_6$], **7**. Used to check for ferromagnetic impurities. Linear fit correlation coefficient R^2 = 0.999374.

Figure S31. Magnetization data at 100 K for (^{H}L)$_2$Fe$_6$(CN)$_6$, **10**. Used to check for ferromagnetic impurities. Linear fit correlation coefficient R^2 = 0.999978.
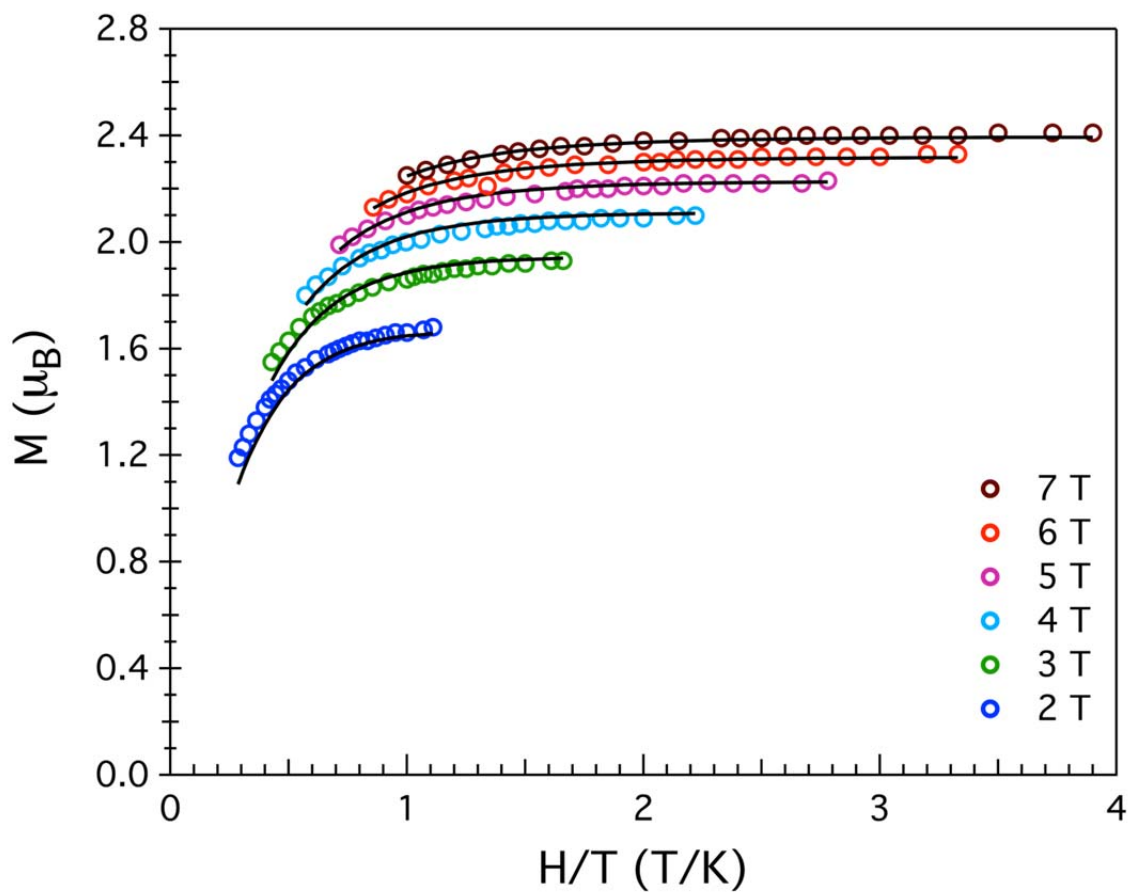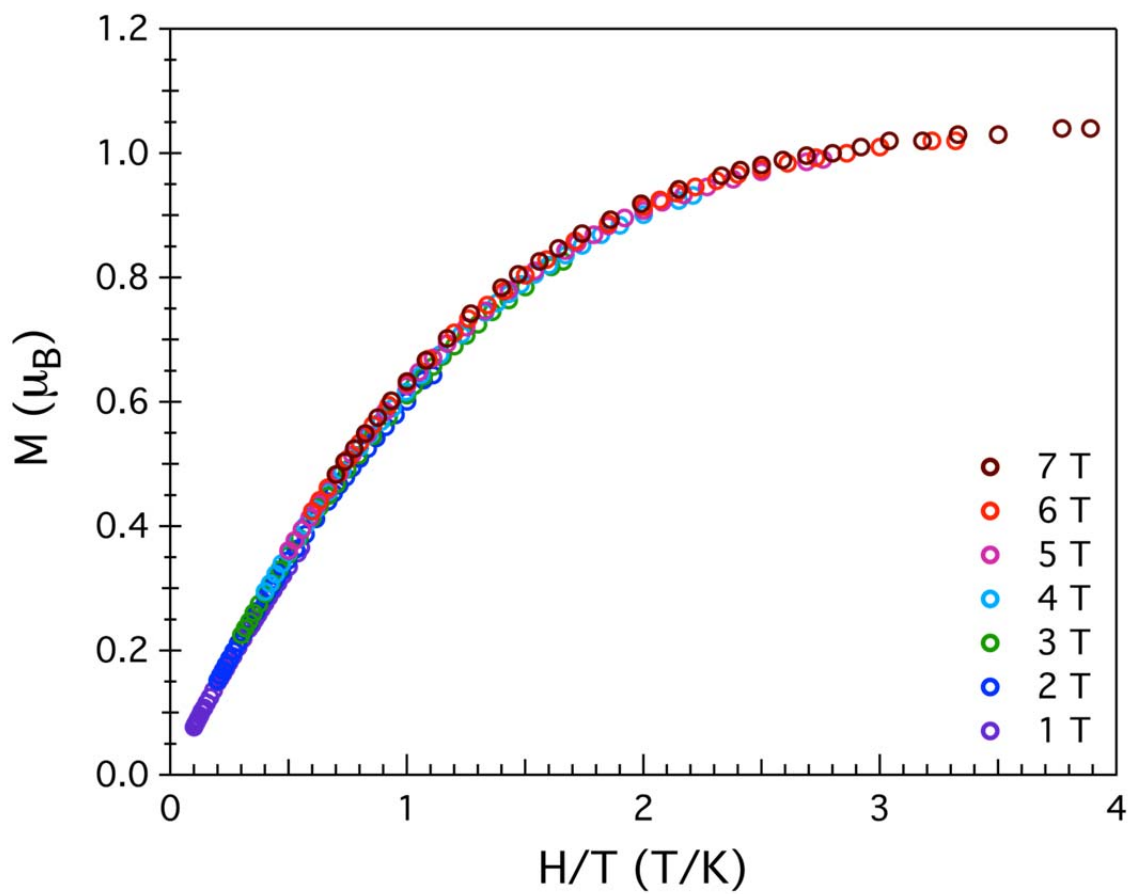
Figure S32. Variable-temperature variable-field reduced magnetization data for
[(^HL)$_2$Fe$_6$(NCMe)$_4$][PF$_6$]$_2$, **1**. Data were collected at each field on heating from 1.8 to 7 K. The
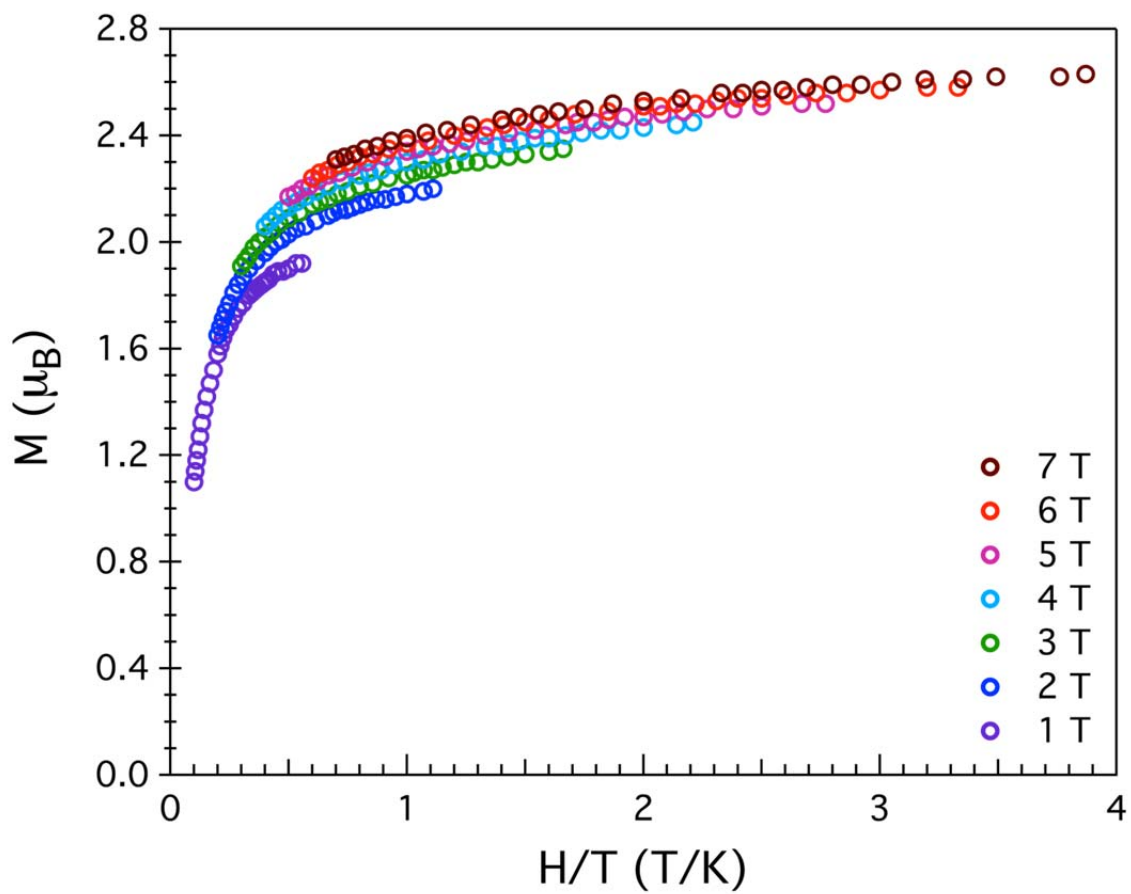continuous lines represent the fit of the data for $S = 2$ with parameters: $D = -21.6$ cm^{-1}, $E/D =$
0.27 and $g = 2.16$.

Figure S33. Variable-temperature variable-field reduced magnetization data for [(^{H}L)$_2$Fe$_6$(NCMe)$_6$][PF$_6$]$_3$, **2**. Data were collected at each field on heating from 1.8 to 10 K.
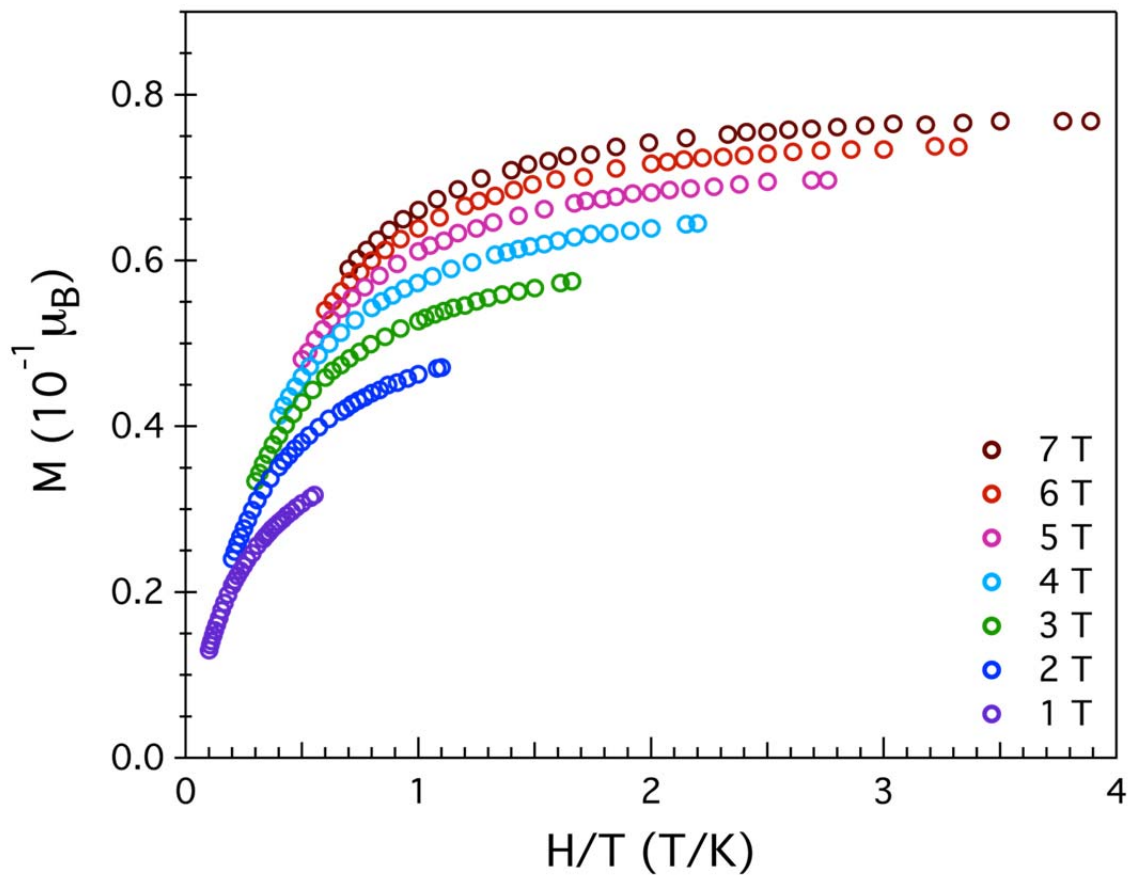
Figure S34. Variable-temperature variable-field reduced magnetization data for [(^{H}L)$_2$Fe$_6$(DMF)$_4$][PF$_6$]$_2$, **4**. Data were collected at each field on heating from 1.8 to 10 K. Although non-superimposable isofield curves are observed the saturation magnitude is rather small. This indicates that even at these temperatures the diamagnetic ground state is not fully reached but a low lying excited state is still accessible within thermal energy.

Figure S35. Variable-temperature variable-field reduced magnetization data for $[(^{H}L)_2Fe_6(DMF)_6][PF_6]_3$, **5**. Data were collected at each field on heating from 1.8 to 10 K.

Figure S36. Variable-temperature variable-field reduced magnetization data for [Bu$_4$N]$_3$[(^{H}L)$_2$Fe$_6$(CN)$_6$], **7**. Data were collected at each field on heating from 1.8 to 10 K. Unfortunately no successful fit could be obtained for this dataset.
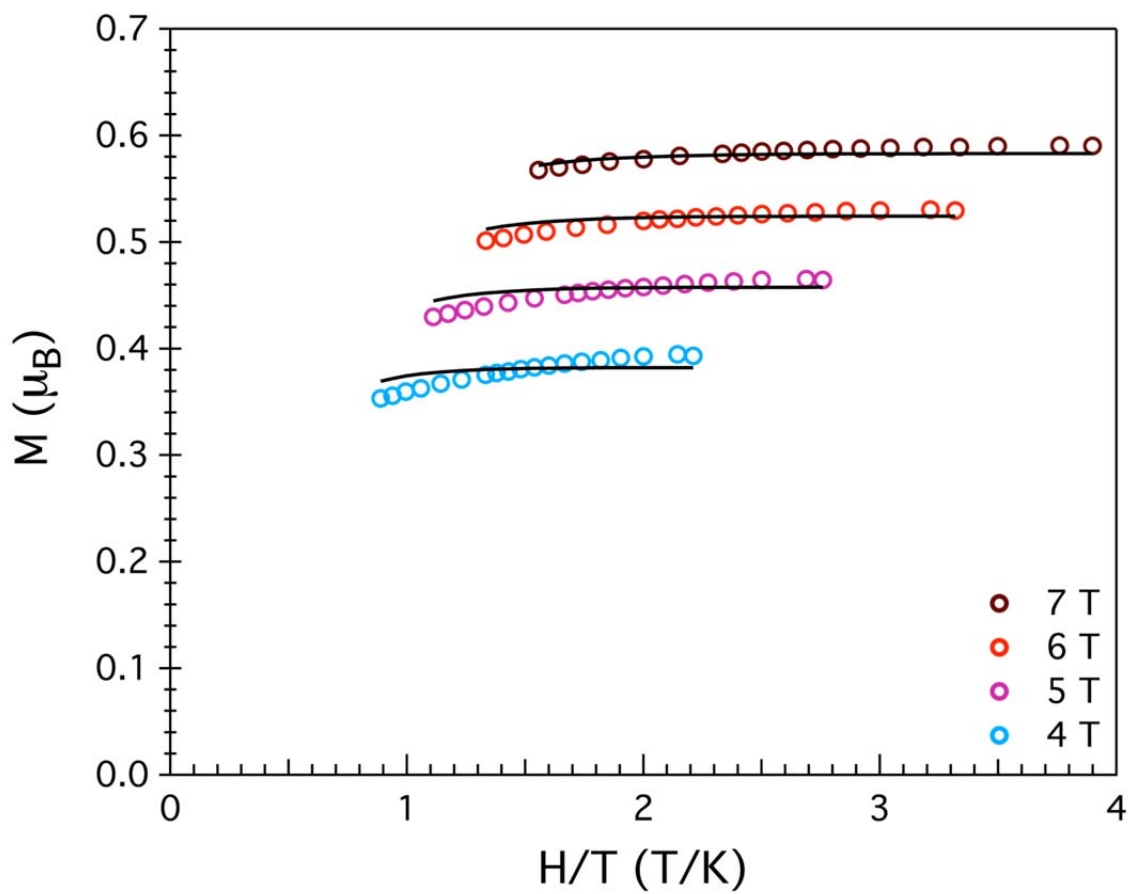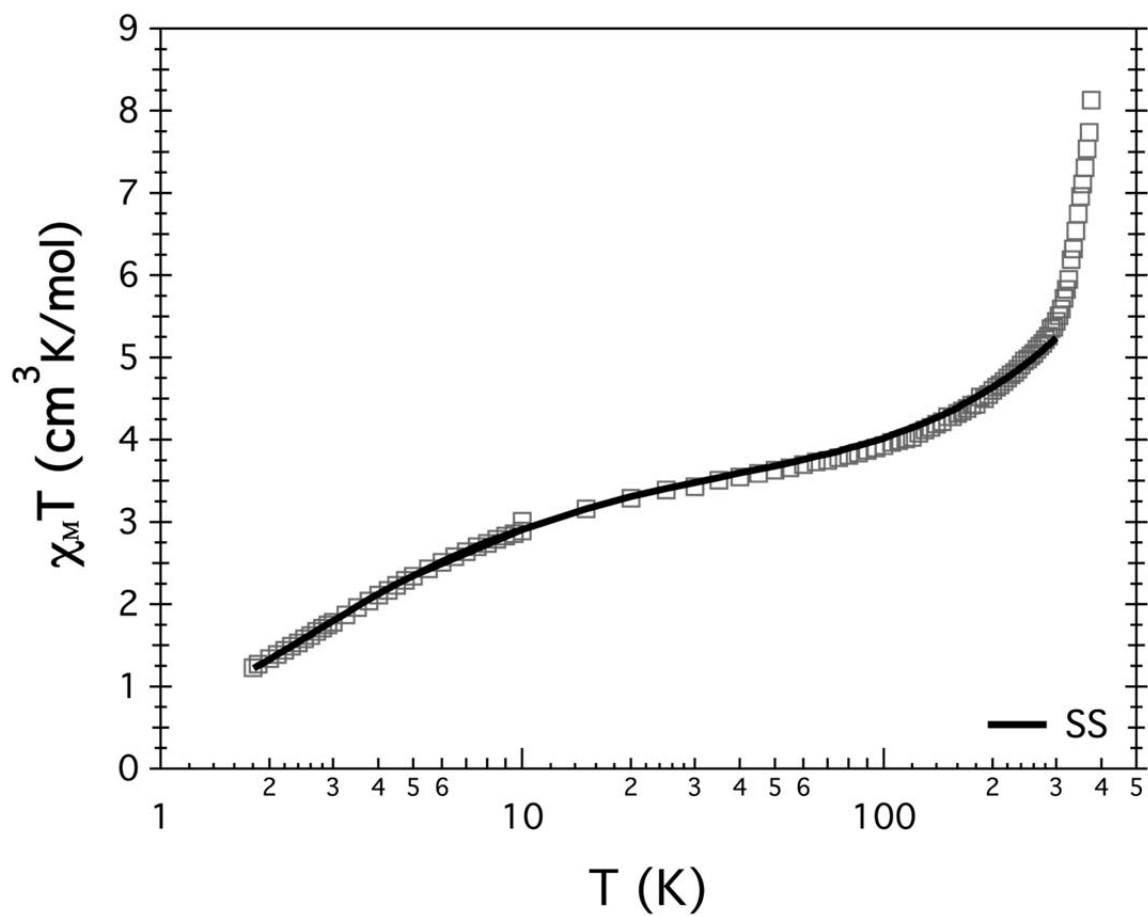
Figure S37. Variable-temperature variable-field reduced magnetization data for $(^HL)_2Fe_6(CN)_6$, **10**. Data were collected at each field on heating from 1.8 to 4.5 K. The continuous lines represent the fit of the data for $S = 1$ and $g = 1.84$ with parameters: $D = -122.4$ cm^{-1}, $E/D = 0.046$.
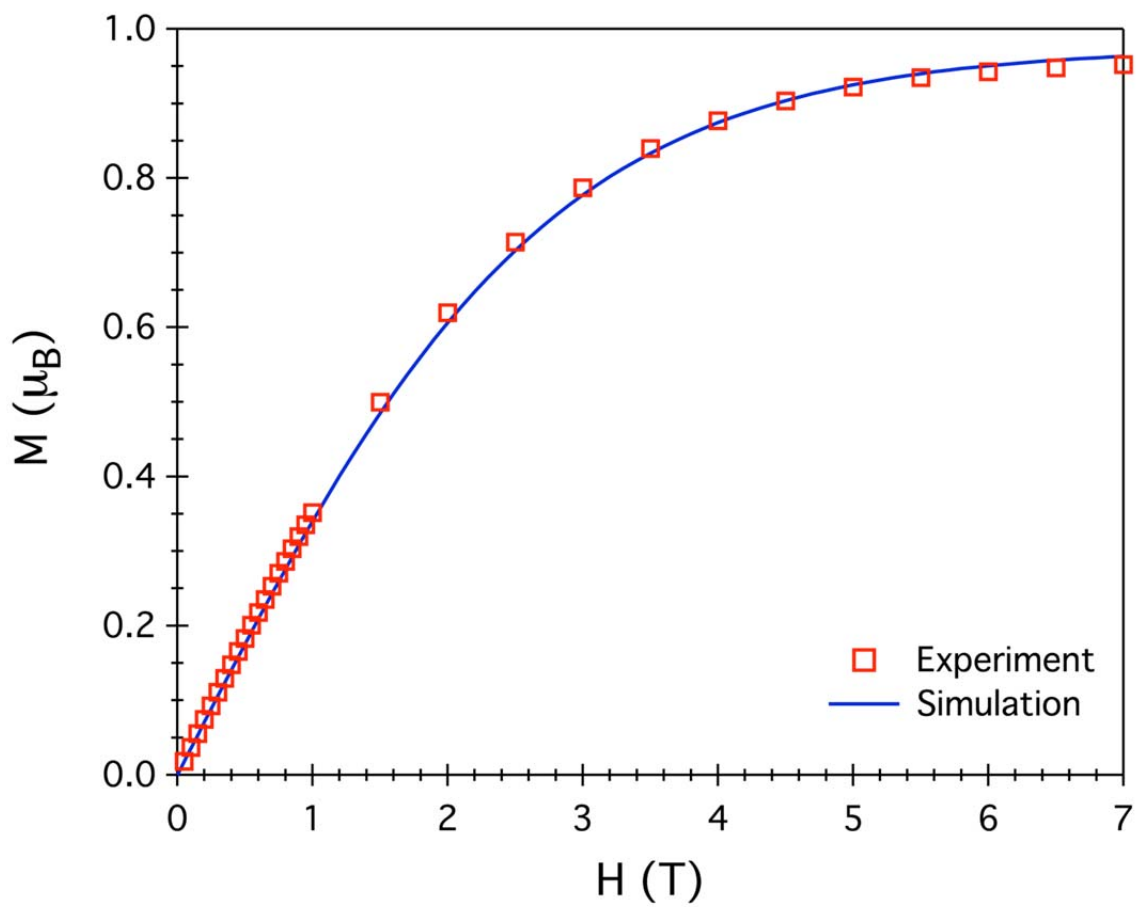
Figure S38. Low temperature magnetization data at 1.8 K form 0 to 7 T for [(^{H}L)$_2$Fe$_6$(NCMe)$_6$][PF$_6$]$_3$, **2**. The continuous blue line corresponds to a Brillouin function simulation using $S = 1/2$ and $g = 1.95$.
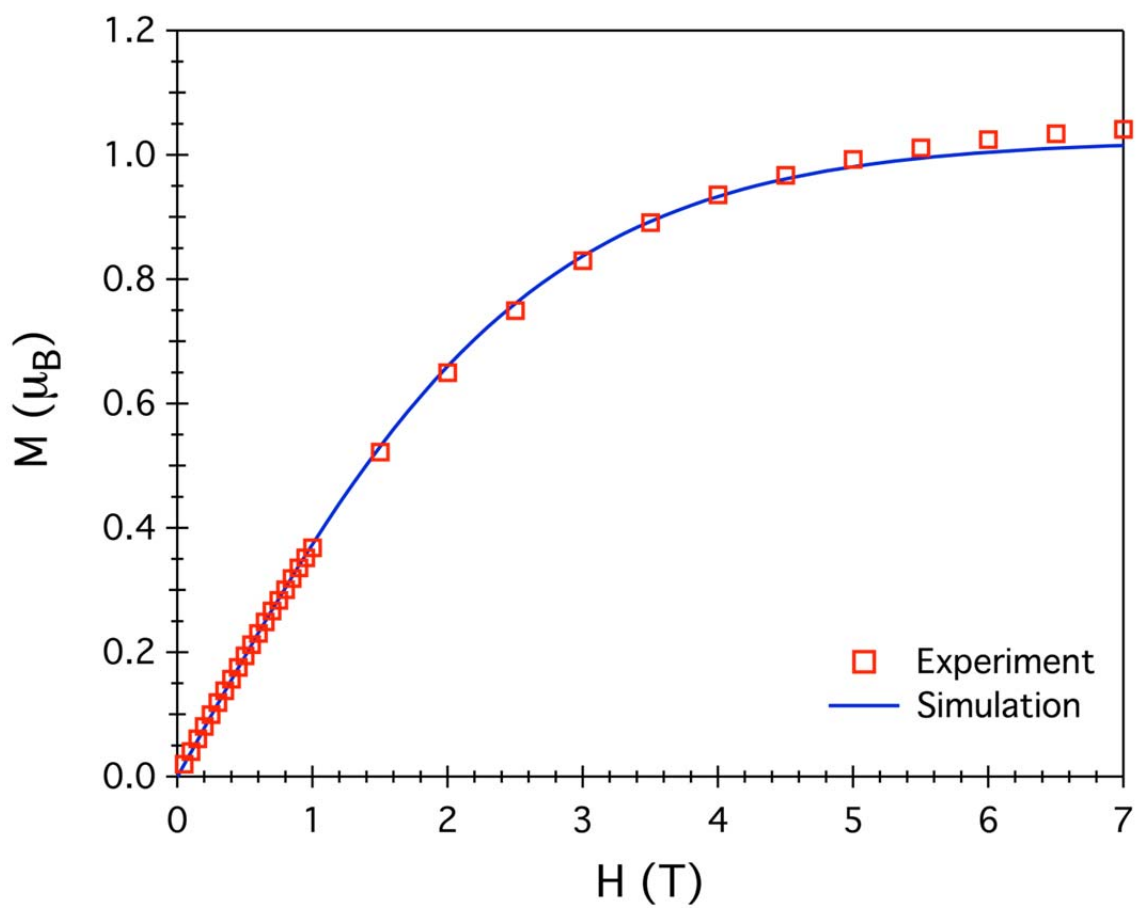
Figure S39. Low temperature magnetization data at 1.8 K form 0 to 7 T for $[(^{H}L)_2Fe_6(DMF)_6][PF_6]_3$, **5**. The continuous blue line corresponds to a Brillouin function simulation using $S = 1/2$ and $g = 2.05$.

Figure S40. Variable-temperature dc magnetic susceptibility data for [(^{H}L)$_2$Fe$_6$(NCMe)$_4$][PF$_6$]$_2$, **1**. Same data as that in Figure 10b but with x-axis expanded logarithmically to better observe the low temperature fit of the data.
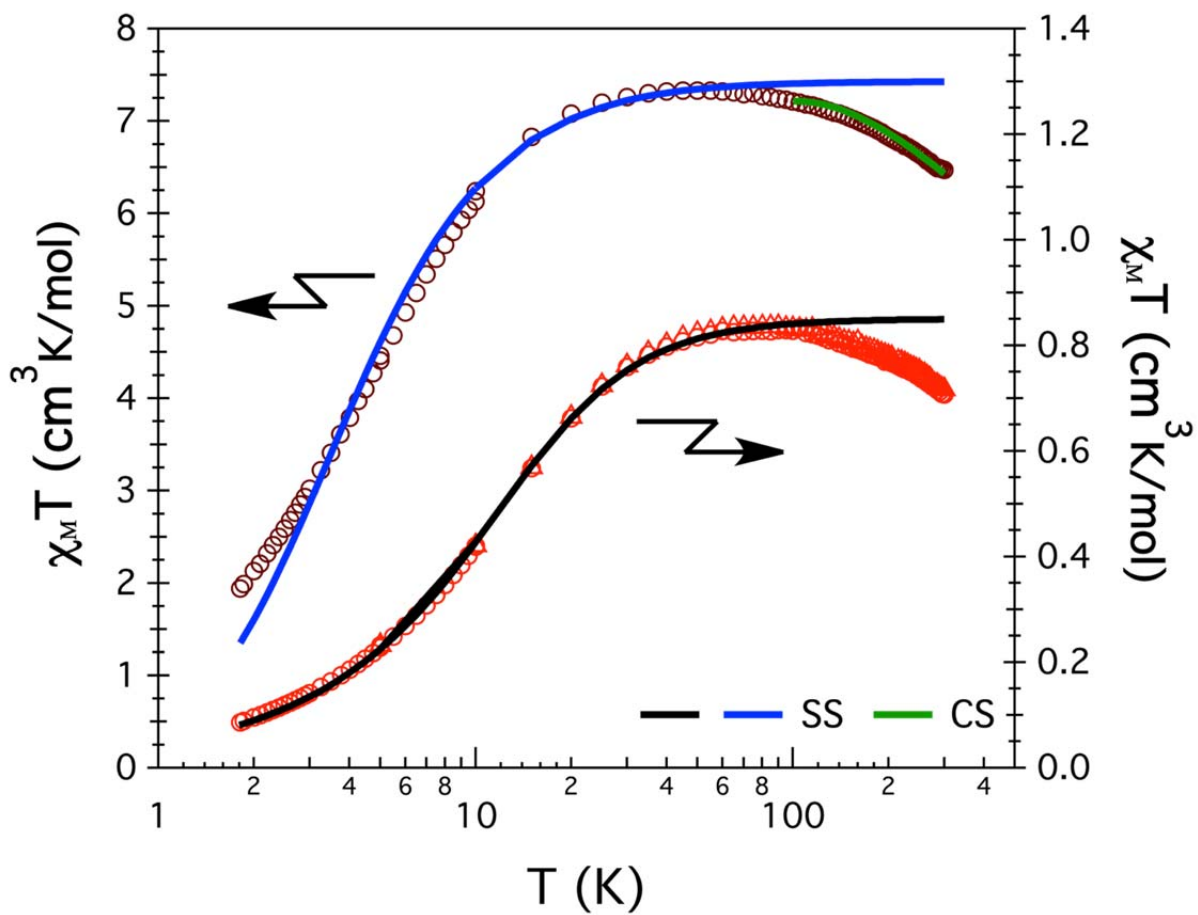
Figure S41. Variable-temperature dc magnetic susceptibility data for $[Bu_4N]_3[(^HL)_2Fe_6(CN)_6]$, **7** maroon; and $[(^HL)_2Fe_6(CN)_6]$, **10** red symbols. Same data as that in Figure 10a but with x-axis expanded logarithmically to better observe the low temperature fit of the data.

(a)

(b)

(c)
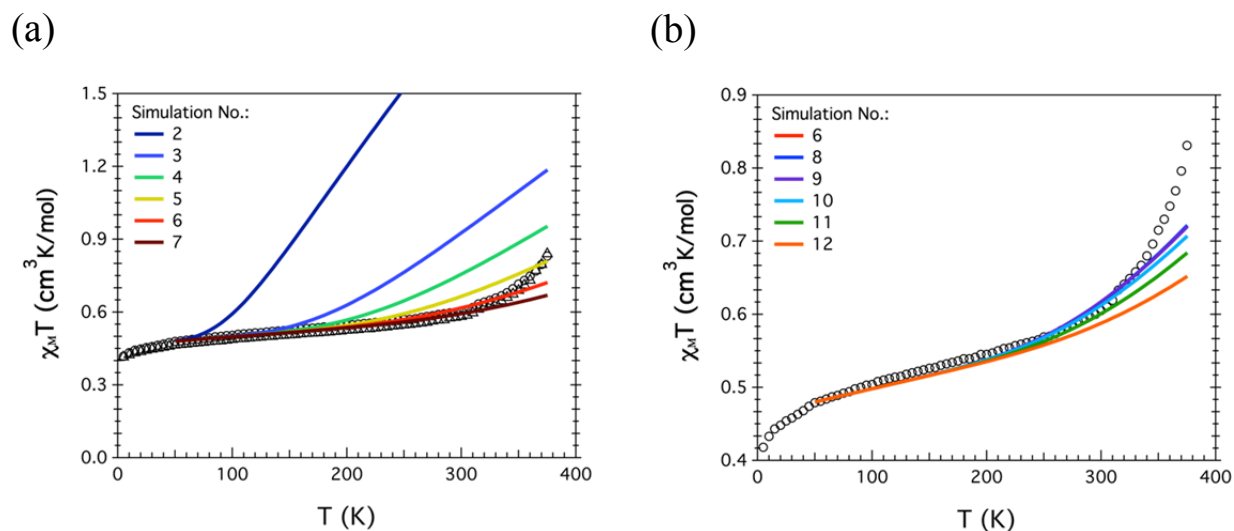
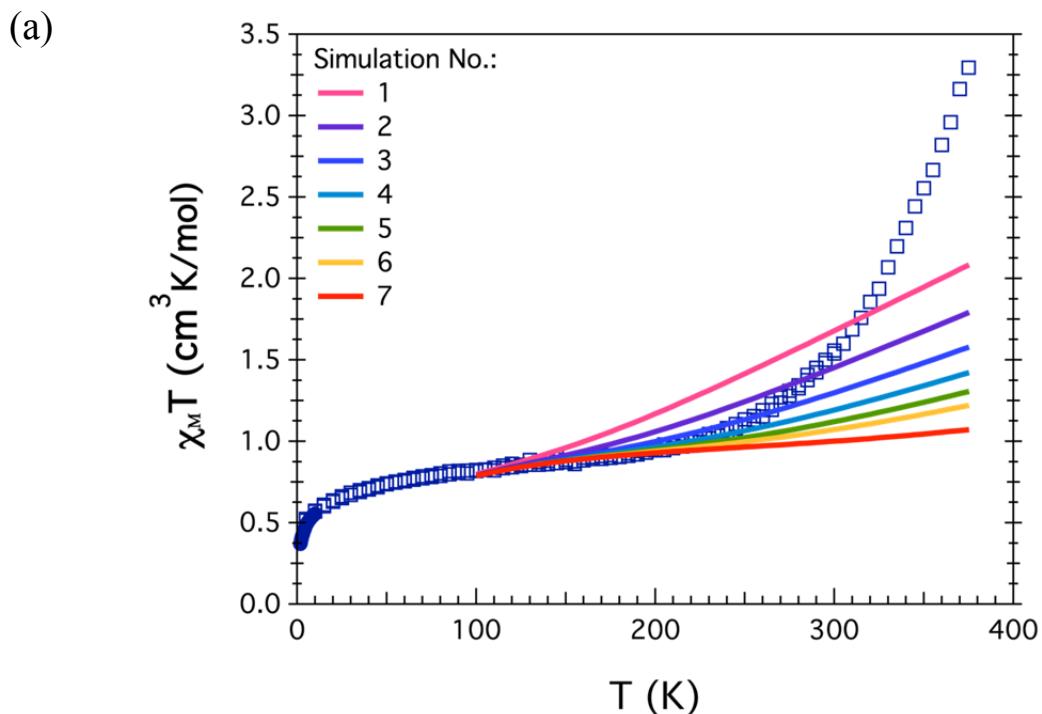| Simulation No.	g	J_{cis} (cm^{-1})	J_{trans} (cm^{-1})	TIP (10^{-6} cm^{3}mol^{-1})	S_a, S_b, S_c
1 (main text)		−315	−390		
2		−100			
3		−200			
4		−250	0		
5		−300			
6	2.22	−350		360	2.5, 2.5, 2.5
7		−400			
8			−100		
9			−200		
10		−350	−300		
11			−400		
12			−500		

Figure S42. Simulations using the coupled spins model of the variable-temperature dc magnetic susceptibility of [(^{H}L)$_2$Fe$_6$(NCMe)$_6$][PF$_6$]$_3$, **2**. The effect of J_{cis} on the simulated curve is shown in (a). All the other parameters were kept constant. In a similar way the effect of J_{trans} on the simulated curve is shown in (b). The parameters for each individual simulation are shown in the table in (c).

(a)

(b)
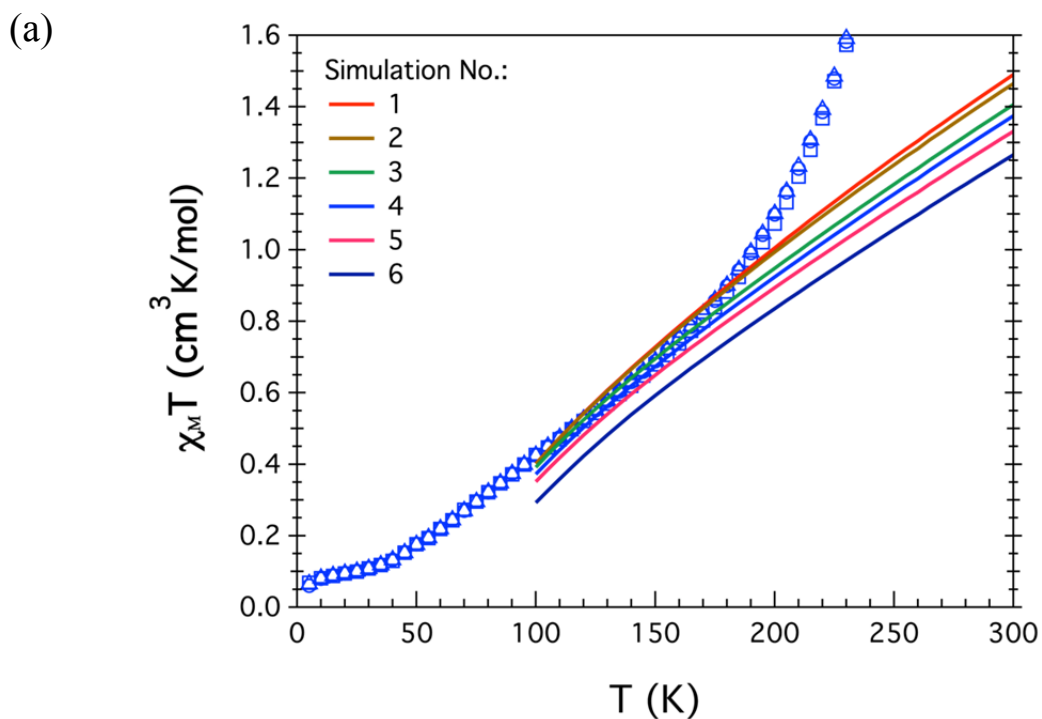
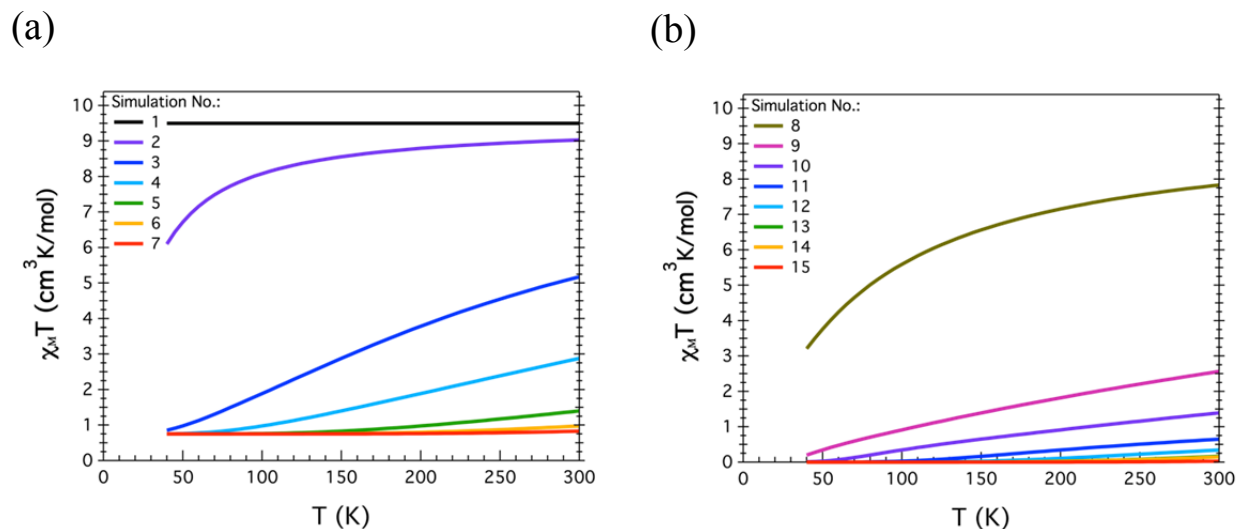| Simulation No.	g	J_{cis} (cm^{-1})	J_{trans} (cm^{-1})	TIP (10^{-6} cm^{3}mol^{-1})	S_a, S_b, S_c
1			0		
2			−20		
3 (main text)	2.05	−95	−60	0	2.5, 2, 2.5
4			−80		
5			−100		
6			−120		

Figure S43. Simulations using the coupled spin model of the variable-temperature dc magnetic susceptibility of [(^{H}L)$_2$Fe$_6$(DMF)$_4$][PF$_6$]$_2$, **4**. J_{cis} was fixed at −95cm^{-1}. The effect of J_{trans} on the simulated curve is shown in (a). All the other parameters were kept constant. The parameters for each individual simulation are shown in the table in (b).

(a)

(b)

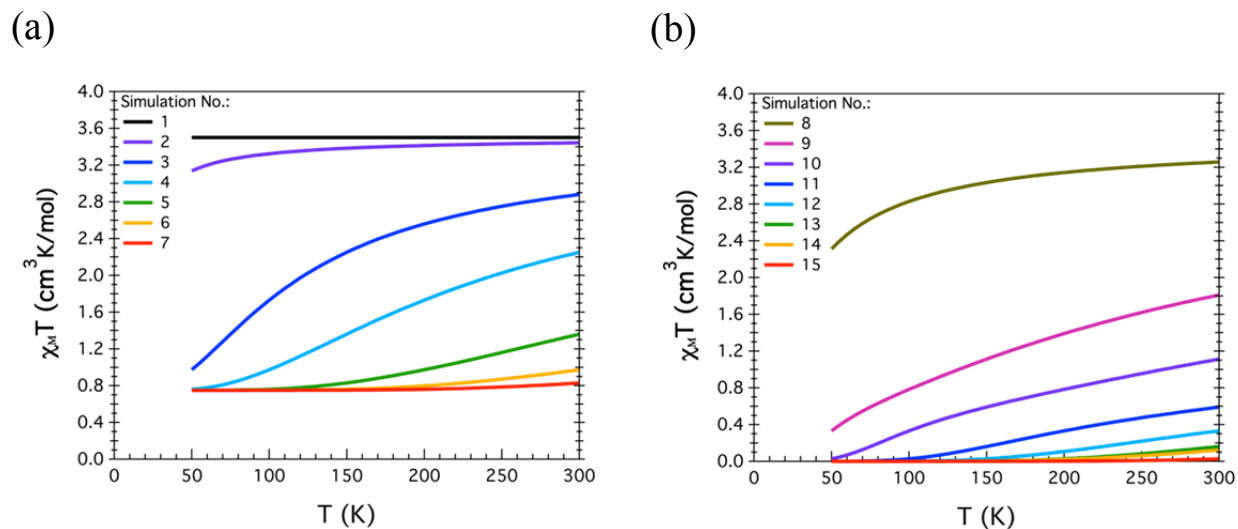| Simulation No.	g	J_{cis} (cm^{-1})	J_{trans} (cm^{-1})	TIP (10^{-6} cm^{3}mol^{-1})	S_a, S_b, S_c
1			−150		
2			−180		
3			−210		
4 (main text)	1.96	−20	−240	0	2.5, 2.5, 2.5
5			−270		
6			−300		
7			−400		

Figure S44. Simulations using the coupled spin model of the variable-temperature dc magnetic susceptibility of [(^{H}L)$_2$Fe$_6$(DMF)$_6$][PF$_6$]$_3$, **5**. J_{cis} was fixed at −20cm^{-1}. The g_{avg} used was that one extracted from the EPR measurement at 3.6 K. The effect of J_{trans} on the simulated curve is shown in (a). All the other parameters were kept constant. The parameters for each individual simulation are shown in the table in (b).

(a)

(b)

(c)

Simulation No.	g	J_{cis} (cm^{-1})	J_{trans} (cm^{-1})	TIP (10^{-6} cm^{3}mol^{-1})	S_a, S_b, S_c
1			0		
2			−5		
3			−50		
4		0	−100		
5			−200		
6			−300		
7			−400		
8	2.0	−5		0	3, 2.5, 2.5
9		−50			
10		−100			
11		−200	0		
12		−300			
13		−400			
14		−400	−400		
15		−600	0		

Figure S45. Simulations using the coupled spins model to account for the diamagnetism observed in [(^{H}L)$_2$Fe$_6$(NCMe)$_6$][PF$_6$]$_4$, **3**; and [(^{H}L)$_2$Fe$_6$(DMF)$_6$][BF$_4$]$_4$, **6**. The effect of J_{trans} on the simulated curve is shown in (a). In a similar way the effect of J_{cis} on the simulated curve is shown in (b). The parameters for each individual simulation are shown in the table in (c).

(a)

(b)

(c)

| Simulation No.	g	J_{cis} (cm^{-1})	J_{trans} (cm^{-1})	TIP (10^{-6} cm^{3}mol^{-1})	S_a, S_b, S_c
1			0		
2			−5		
3			−50		
4		0	−100		
5			−200		
6			−300		
7			−400		
8	2.0	−5		0	1.5, 1.5, 1
9		−50			
10		−100			
11		−200	0		
12		−300			
13		−400			
14		−400	−400		
15		−600	0		

Figure S46. Simulations using the coupled spins model to account for the diamagnetism observed in [Bu$_4$N]$_2$[(^{H}L)$_2$Fe$_6$(CN)$_6$], **8**. The effect of J_{trans} on the simulated curve is shown in (a). In a similar way the effect of J_{cis} on the simulated curve is shown in (b). The parameters for each individual simulation are shown in the table in (c).
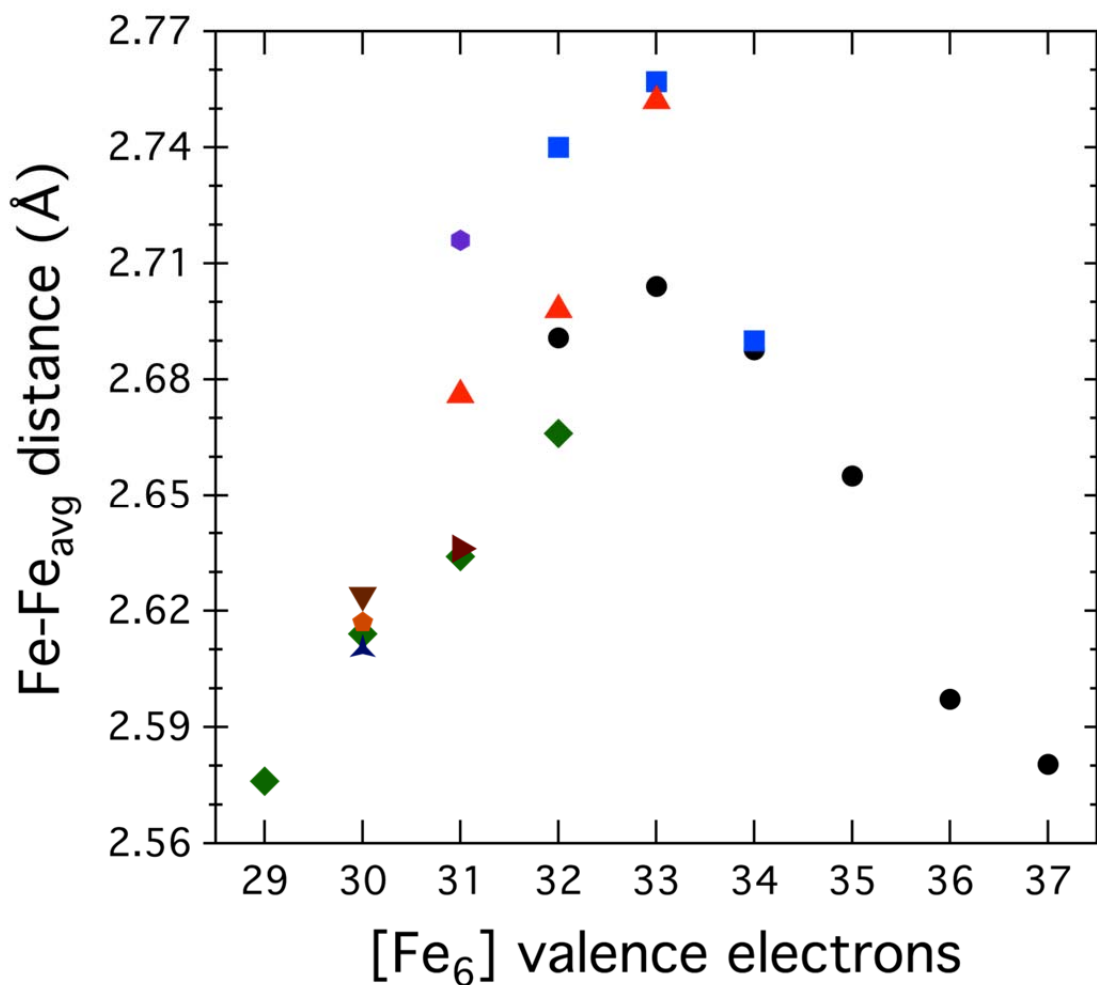
Figure S47. Comparison of the average Fe–Fe distances of the clusters synthesized in this work and the literature precedent. For the clusters reported by this laboratory: valence electrons (VE) = $36 - n$. This work and previous[6b]: $[(^HL)_2Fe_6(NCMe)_m]^{n+}$ solid black circles, ● ($n = -1$ to 4); $[(^HL)_2Fe_6(DMF)_m]^{n+}$ solid blue squares, ■ ($n = 2$ to 4); $[(^HL)_2Fe_6(CN)_6]^{n-6}$ solid red triangles, ▲ ($n = 3$ to 6). For literature comparisons: VE = $32 - n$; $[Fe_6(\mu^3\text{-}E)_8(PEt_3)_6]^{n+}$ (E, n): ▼ (S, 2);[12] ⬠ (S, 2);[13] ▶ (S, 1);[14] ▲ (S, 2);[15] ◆ (S, 0 to 3);[16] ● (Se, 1).[17]

References.

(1) Klose, A.; Solari, E.; Floriani, C.; Chiesivilla, A.; Rizzoli, C.; Re, N. *J. Am. Chem. Soc.* **1994**, *116*, 9123.

(2) D'alessandro, D. M.; Keene, F. R. *Chem. Soc. Rev.* **2006**, *35*, 424.

(3) (a) Hush, N. S. In *Prog. Inorg. Chem.*; John Wiley & Sons, Inc.: 1967, p 391. (b) Hush, N. S. *Electrochim. Acta* **1968**, *13*, 1005.

(4) Brunschwig, B. S.; Sutin, N. *Coord. Chem. Rev.* **1999**, *187*, 233.

(5) Brunschwig, B. S.; Creutz, C.; Sutin, N. *Chem. Soc. Rev.* **2002**, *31*, 168.

(6) (a) Harris, T. D.; Zhao, Q. L.; Hernández Sánchez, R.; Betley, T. A. *Chem. Commun.* **2011**, *47*, 6344. (b) Zhao, Q. L.; Harris, T. D.; Betley, T. A. *J. Am. Chem. Soc.* **2011**, *133*, 8293.

(7) Aromi, G.; Knapp, M. J.; Claude, J. P.; Huffman, J. C.; Hendrickson, D. N.; Christou, G. *J. Am. Chem. Soc.* **1999**, *121*, 5489.

(8) Kambe, K. *J. Phys. Soc. Jpn.* **1950**, *5*, 48.

(9) Kahn, O. *Molecular magnetism*; VCH, 1993.

(10) Eames, E. V.; Harris, T. D.; Betley, T. A. *Chem. Sci.* **2012**, *3*, 407.

(11) Chilton, N. F.; Anderson, R. P.; Turner, L. D.; Soncini, A.; Murray, K. S. *J. Comput. Chem.* **2013**, *34*, 1164.

(12) Cecconi, F.; Ghilardi, C. A.; Midollini, S. *J. Chem. Soc. Chem. Comm.* **1981**, 640.

(13) Agresti, A.; Bacci, M.; Cecconi, F.; Ghilardi, C. A.; Midollini, S. *Inorg. Chem.* **1985**, *24*, 689.

(14) Cecconi, F.; Ghilardi, C. A.; Midollini, S.; Orlandini, A.; Zanello, P. *J. Chem. Soc. Dalton Trans.* **1987**, 831.

(15) Bencini, A.; Ghilardi, C. A.; Midollini, S.; Orlandini, A.; Russo, U.; Uytterhoeven, M. G.; Zanchini, C. *J. Chem. Soc. Dalton. Trans.* **1995**, 963.

(16) Goddard, C. A.; Long, J. R.; Holm, R. H. *Inorg. Chem.* **1996**, *35*, 4347.

(17) Cecconi, F.; Ghilardi, C. A.; Midollini, S.; Orlandini, A. *Inorg. Chim. Acta* **1997**, *254*, 387.